Supplementary Material for

Estimating Commercial Cooking Contribution to Urban $PM_{2.5}$ and O_3 with a Refined Emission Inventory from a Unified Online-Source Framework

Yingzhi Yuan[1], Yun Zhu[1], Ji-cheng Jang[1], Dian Ding[1], Zhaoxin Dong[1], Meijun Chen[1], Bin Zhao[2,3], Jiaqian Hu[1], Xiansheng Shi[1]*

[1] Guangdong Provincial Key Laboratory of Atmospheric Environment and Pollution Control, School of Environment and Energy, South China University of Technology, Guangzhou Higher Education Mega Center, Guangzhou 510006, China

[2] State Key Joint Laboratory of Environment Simulation and Pollution Control, School of Environment, Tsinghua University, Beijing 100084, China

[3] State Environmental Protection Key Laboratory of Sources and Control of Air Pollution Complex, Beijing 100084, China

* Correspondence to: Yun Zhu (zhuyun@scut.edu.cn)

This Supplementary Material contains 65 pages, 7 sections, 10 tables and 23 figures.

Table of Contents

Tables:

Figures:

Section S1. The structure of the online oil fumes monitoring system

The structure of the online oil fumes monitoring system was shown in **Fig. S1**. The oil fumes were firstly extracted into the detector by a pump-driven sampling unit and then analyzed by the integrated analysis module, with $PM_{2.5}$ and non-methane VOCs (VOCs) concentrations based on the light scattering principle and electrochemical detection principles respectively. The switching state and operating current of purifying equipment

and wind turbine were also recorded by the sensor. Thereafter, these data would be transferred to the monitoring host for integration and regularly uploaded to the data management platform for display in a cloud platform per ten minutes. The hardware of the system was shown in **Fig. S2**.

The operation principle of the $PM_{2.5}$ concentration analysis was shown in **Fig. S3**. The particles in the oil fumes caused the light scattering phenomenon under the illumination of LED lights. A pulse light signal was accepted on the photoelectric detector and accordingly transferred to an electrical signal by the photosensitive resistance to calculate the generated pulse number. The pulse was directly proportional to the $PM_{2.5}$ concentration. Therefore, the determination of $PM_{2.5}$ concentration can be rapidly and continuously obtained by constructing the relationship between $PM_{2.5}$ concentration and pulse light signal. The detector had been calibrated based on the balance weighing principle before application.

The operational principle of electrochemical detection for VOCs in cooking oil fumes was illustrated in **Fig. S6**. The cooking oil fumes were initially filtered through a membrane to remove particulate matter and interfering components. The treated gas was subsequently diffused into the sensor through a permeable membrane, reaching the surface of the working electrode where oxidation or reduction reactions occur under the catalytic action of specific catalysts, such as metal oxides. Electrons were released during this process, generating a current signal proportional to gas concentration. This signal was then

calibrated and converted into non-methane VOCs concentration values through standardized procedures.

Section S2. Sampling and analysis method

A standardized sampling protocol was implemented with the sampling probe positioned at the central axis of the flue to avoid vortex interference (**Fig. S1**). The collection of VOCs was performed according to US. EPA *TO-14* (Center for Environmental Research Infromation Office of Research and Development U.S. Environmental Protection Agency Cincinnati, 1999), one of the standard sampling procedures, using electropolished stainless steel canisters with a sample volume capacity of 2 L. During sampling, a needle valve was employed to maintain the flow rate of 300 $mL \cdot min^{-1}$ with a duration of 10 min, and a particulate filter was installed upstream of the canister to prevent particulate matter from obstructing the needle valve and contaminating the canister interior. Before sampling, the canisters were subjected to leak testing, followed by several cycles of pressurization and evacuation with N_2 for thorough cleaning. After sampling, the canister valve was closed and a protective cap was secured to prevent the ingress of particulate matter during handling and transport.

The qualitative and quantitative analysis of VOCs was performed using a preconcentrator (Entech 7100 Preconcentrator, Entech Instruments Inc., California, USA) coupled with a Gas Chromatograph/Mass Selective Detector/Flame Ionization Detector/Electron Capture Detector (GC-MSD/FID/ECD, 6890 GC/Agilent 5973N)

system (**Fig. S7**). The C2 (ethane, ethylene, acetylene) and C3 (propylene, propane) non-methane hydrocarbons (NMHCs) were analyzed through FID detector while C4-C10 NMHCs were analyzed through MSD detector. The compound identification was based on chromatographic retention times and mass spectra, and the quantification was achieved through the external standard method, comparing the chromatographic peak areas of the samples to those of standard reference materials. The calibration curves were established through diluting the Photochemical Assessment Monitoring Stations (PAMS) standard mixture (57 VOCs) with concentrations of 100 ppbv to 0.5, 1, 5, 15, and 30 ppbv. Each compound was calibrated with these different concentration levels of the standard mixtures along with a blank sample, with the linear correlation coefficients (R^2) exceeding 0.99. **Table S2** lists the specific VOCs detected in this study.

The collection of gaseous oxygen-containing volatile organic compounds (OVOCs) was achieved through a two-stage DNPH-coated silica gel cartridge (Sep-Pak DNPH-Silica Cartridge, Waters, MSA). Cooking oil fumes were directed through a potassium iodide (KI)-coated ozone scrubber column for particulate matter removal and subsequently adsorbed onto DNPH solid-phase extraction cartridges at a flow rate of 1.5 L/min for 10 minutes. Post-sampling, DNPH cartridges were packed tightly with tin paper or aluminum foil and stored at low temperature (lower than 4°C) for no more than a week. The qualitative and quantitative analysis of OVOCs was performed using a High-Performance Liquid Chromatography (HPLC) system (HP1200, Aligent, USA) equipped with an Agilent SB-

C18 reversed-phase column for separation and an UV detector for detection (**Fig. S8**). The identifiable OVOC species include 12 types of carbonyl compounds (**Table S2**). Calibration curves for each compound were established through analysing a series of standard solutions with 8 concentrations ranging from 0.05 to 20 μg·mL^{-1}, with R^2 exceeding 0.999.

The $PM_{2.5}$ was collected on pre-fired (450 ℃, 6h) quartz-fiber filters (47 mm, Whatman, Mainstone, UK) at a flow rate of 16.7 L·min^{-1} for 60 min. All samples were stored under refrigeration at 2 ℃ before analysis. The mass concentrations of $PM_{2.5}$ were determined gravimetrically by weighing the filters before and after sampling. Prior to weighing, all filters were equilibrated for at least 24 hours in a chamber maintained at 2°C and 40% relative humidity (RH). Subsequently, in a balance room controlled at 25°C and below 55% RH, the quartz filter membranes containing collected atmospheric particulate matter were weighed using a microbalance (Cahn C-35, ±0.1 μg). The $PM_{2.5}$ mass concentrations were then calculated according to the **Eqs. (S1)** to **(S2)**.

$$PM_{2.5}\left(\frac{\mu g}{m^3}\right) = \frac{(w_2 - w_1) \times 10^6}{V_n} \quad (S1)$$

$$V_n = Q \times \frac{P_2 \times T_n}{P_n \times T_2} \times t \times 60 \quad (S2)$$

Where, W_1 and W_2 (g) are the mass of the quartz filter before and after sampling, respectively. V_n (m^3) is the total sampling volume under standard conditions. Q ($m^3 \cdot min^{-1}$) is the average sampling flow rate. P_n and P_2 (kPa) are the ambient pressure under standard

conditions and during sampling, respectively. T_n and T_2 (K) are the ambient temperature under standard conditions and during sampling, respectively.

Section S3. Concentrations and speciation of commercial cooking-emitted VOCs across Cuisine Types

Fig. S9 summarizes the average mass concentrations of VOCs and $PM_{2.5}$ measured from six cooking categories, including Cantonese cuisine (CC), Sichuan-Hunan cuisine (SHC), Chinese fast-food (CFF), Non-Chinese cuisine and barbecue (NCB), other Chinese cuisine (OCC) and institutional canteens. The VOCs concentrations were 12975.2, 6830.1, 6130.3, 2274.9, 42242.2, and 2776.3 μg/m^3, respectively, while the corresponding $PM_{2.5}$ concentrations were 6195.1, 1099.2, 2473.8, 649.6, 555.5 and 329.0 μg/m^3. SHC, CFF and CC were identified as the top three emitters for both VOCs and $PM_{2.5}$, which was consistent with previous research findings (Liang et al., 2022). This observation can be explained by the frequent use of high-temperature cooking techniques such as stir-frying and deep-frying in these three culinary styles, which typically generate higher emission intensities compared to other cooking methods.

Fig. S10 presents the contributions of VOCs chemical categories to total VOCs for each cuisine type. Consistent with earlier observations (Huang et al., 2020; Sun et al., 2022), alkanes dominated the VOCs composition in most cuisines, accounting for 82.67%, 77.10% and 80.39% in SHC, CFF and NCB, respectively. These alkanes were primarily short-chain species such as propane, n-butane, and isobutane, which may originate from thermal

cracking of oils and fats at high temperatures and minor leakage of cooking fuels such as liquefied petroleum gas (LPG). Notably, NCB exhibited a high proportion of n-pentane (13.42%), likely associated with the incomplete combustion of dripped fat during open-flame grilling (Schauer et al., 1999). In contrast, canteen emissions were characterized by a markedly oxygenated profile, with O-VOCs contributing 66.69% of total VOCs and acetaldehyde, vinyl acetate, ethyl acetate, and acetone identified as the dominant species. This O-VOC-rich composition likely continues large-pot cooking and repeated heating of cooking oils, which promotes oxidation/hydrolysis and generates substantial quantities of low-molecular-weight aldehydes, ketones, and esters (Wang et al., 2018). In addition, canteens are typically fueled by natural gas and electric cookers, with limited use of LPG. This fuel mix may reduce LPG-related fugitive emissions of light alkanes (e.g., propane and butanes), thereby increasing the relative contribution of oxygenated VOCs formed during cooking processes. OCC showed a diversified speciation pattern, with alkanes as a major component together with notable fractions of acetaldehyde and 1-butene, which likely reflected the heterogeneity of cooking methods included in this category. Overall, alkanes and O-VOCs consistently dominated the measured VOCs profiles across all cuisine types. However, the major contributing species varied substantially among cuisines, indicating distinct source fingerprints associated with different cooking practices.

Section S4. The calibration function establishment for $PM_{2.5}$

To establish a functional relationship between OOFM data and sampled concentrations for the calibration of online $PM_{2.5}$ concentrations, sampled $PM_{2.5}$ concentrations were paired with timestamp-matched online monitoring $PM_{2.5}$ concentrations, with two validation samples reserved. Following Cook's distance calculation across the $PM_{2.5}$ dataset, the second group of data was removed as an outlier (**Fig. S13**). Least squares regression was then applied to the retained sample data, yielding the calibration curve presented in **Fig. S14c**. Consistent with initial VOCs test-data results, elevated relative errors were observed in low-concentration $PM_{2.5}$ samples (**Table S4**), reaching a maximum of 25.96% which exceeded the 20% tolerance threshold. Consequently, training set residuals were analyzed and fitted to generate a residual fitting function (**Fig. S14d**). The second derivative of this function was subsequently calculated to identify the point of maximum curvature, with it driven at 820 $\mu g/m^3$ established as the partitioning threshold between low-concentration and high-concentration regimes. Segmented least squares regression was subsequently performed within each concentration regime (**Fig. S15b**). The validation testing of the optimized fitting demonstrated marked error reduction, with the maximum relative error decreasing from 25.96% to -3.18%. All validation samples exhibited relative errors below 20%, confirming significantly improved accuracy in the low-concentration region.

Section S5. Method of estimating emissions from commercial cooking without OOFM data

The emission estimations of VOCs and $PM_{2.5}$ from commercial cooking without OOFM data were processed following **Eq. (S3)**. Temporal allocation was performed by referring to the hourly and daily coefficients in the technical manuals. Given insignificant monthly variations in commercial cooking emissions (Yuan et al., 2023), monthly allocation coefficients were uniformly set to 0.083 (1 divided by 12).

$$E_i = \sum_j EF_i \times r_j \times M \times N_j \times V_j \times T_j \times 10^{-9} \quad \text{(S3)}$$

where, *i* is one of the two pollutants (VOCs and $PM_{2.5}$). *j* is the scale of restaurants (Large, medium and small). *E* is the emissions (t/a) of pollutant *i*. *EF* is the emission factor (mg/m^3) for five pollutants of cooking listed in the *Technical Manual for the preparation of city-level air pollutant emission inventory 2024 (Technical Manual)*. The values were 5.60 and 6.40 for VOCs and $PM_{2.5}$, respectively. *r* is the proportion of the scale *j* restaurants. In reference to the previous study of Huang et al. (2013), the proportion of different business scales were set as 0.09, 0.15 and 0.77 for large, medium and small scales, respectively. *M* is the total number of the catering enterprises in Guangdong Province in 2023 obtained from the POI data. *N* is the number of stove heads. The *N* value of large, medium and small restaurants in the *Technical Manual* were 1 - 2, 3 - 5 and ≥ 6, respectively. Medium values were adopted for small (1.5) and medium (4) scales; as for the large scale, we used the investigated value (7.1) referring to the work of Jin et al. (2021). *V* is the oil fumes gas discharge rate of each stove head. According to the *Technical Manual*, the *V* value of large, medium and small restaurants were 2500, 2000 and 1500 m^3/h, respectively. *T* is the working hours. For large, medium and small scales, *T* value were set as 2000,1800 and

1600 hours per year referring to the *Technical Manual*, respectively. 10^{-9} was used to convert the unit of emissions from grams to tons (t).

Section S6. Formulas of statistic indicators for the WRF-CMAQ validation

Normalized Mean Bias (NMB)

$$NMB = \frac{\sum_{i=1}^{N}(S_i - O_i)}{\sum_{i=1}^{N} O_i} \quad \text{(S4)}$$

Correlation coefficient (R)

$$R = 1 - \frac{\sum_{i=1}^{N}(S_i - \bar{S})(O_i - \bar{O})}{\sqrt{\sum_{i=1}^{N}(S_i - \bar{S})^2 \sum_{i=1}^{N}(O_i - \bar{O})^2}} \quad \text{(S5)}$$

where, N referred to the number of time series samples. S_i and O_i were the simulated and observed values, respectively, of sample i. $\bar{S}$ and $\bar{O}$ represented the mean of all values over time series simulated and observed respectively.

Section S7. The calculation of SMAT-CE Tool

In order to improve the accuracy of pollutant concentration simulation results, the SMAT-CE Tool developed by the U.S. Environmental Protection Agency (U.S. EPA) was used to realize the data fusion of air quality model simulation results and air quality monitoring concentration. The simulated data of the control scenario were adjusted by using the monitoring and model data of the base scenario together with the gridded response factors constructed based on the simulation results between the base and control scenarios. In SMAT-CE, the eVNA interpolation algorithm, which can reflect the performance of monitoring data and retain the gradient characteristics of simulation results, was used to process the simulation results of the base scenarios. Detailed formulas were given in **Eqs. (S6)** to **(S8)**.

$$GridCell_{E,control} = GridCell_{E,base} * RRF_E \quad \text{(S6)}$$

$$GridCell_{E,base} = \sum_{i=1}^{m} Weight_i * Monitor_i * \frac{Model_{E,base}}{Model_{i,base}} \quad \text{(S7)}$$

$$RRF_E = \frac{\sum_{j=1}^{n} \frac{Model_{j,control}}{Model_{j,base}}}{n} \quad \text{(S8)}$$

where, $GridCell_{E,control}$ represented the adjusted simulation results of grid E in the control scenario. $GridCell_{E,base}$ represented the adjusted simulation results of grid E in the base scenario. RRF_E was the response factor of grid E, which was calculated by averaging the ratio of the simulation results between the base and control scenario in grid E and its surrounding n grids. m was the number of atmospheric monitoring stations near grid E. $Weight_i$ was the inverse distance weighted interpolation weight of the adjacent station i. $Monitor_i$ was the observation of the adjacent station i. $Model_{E,base}$ was the simulation result of grid E in the base scenario. $Model_{i,base}$ was the simulation result of the grid where station i was located in the base scenario.

Table S1. Sampling information for each cuisine type

Cuisines	Enterprises numbers	Sample sizes		Features
		VOCs	$PM_{2.5}$	
Cantonese cuisine (CC)	11	33	10	Steaming, Stir-frying
Sichuan-Hunan cuisine (SHC)	1	3	1	High-Heat Stir-frying, Braising
Chinese fast food (CFF)	3	9	3	Rapid Stir-frying, Deep-frying
Non-Chinese and barbecue (NCB)	4	12	3	Grilling, Pan-frying, Roasting
Other Chinese cuisine (OCC)	2	6	2	Wok Stir-frying, Braising/Stewing

Canteens	4	12	4	Large-batch Stir-frying, Boiling/Stewing (Scaled production methods)

Table S2. List of the detected common VOCs species (No. 1-58) and OVOCs species (No. 59-70).

Number	Species	Number	Species
1	Ethane	36	trans-2-Pentene
2	Propane	37	cis-2-Pentene
3	Isobutane	38	Isoprene
4	n-Butane	39	1-Hexene
5	Isopentane	40	Acetylene
6	n-Pentane	41	Benzene
7	2,2-Dimethylbutane	42	Toluene
8	Cyclopentane	43	Ethylbenzene
9	2,3-Dimethylbutane	44	m,p-Xylene
10	2-Methylpentane	45	o-Xylene
11	3-Methylpentane	46	Styrene
12	n-Hexane	47	Isopropylbenzene
13	Cyclohexane	48	n-Propylbenzene
14	Methylcyclohexane	49	m-Ethyltoluene
15	Methylcyclopentane	50	p-Ethyltoluene
16	2,4-Dimethylpentane	51	1,3,5-Trimethylbenzene
17	2-Methylhexane	52	o-Ethyltoluene
18	2,3-Dimethylpentane	53	1,2,4-Trimethylbenzene
19	3-Methylhexane	54	1,2,3-Trimethylbenzene
20	2,2,4-Trimethylpentane	55	m-Diethylbenzene
21	n-Heptane	56	p-Diethylbenzene
22	2,3,4-Trimethylpentane	57	Vinyl Acetate
23	2-Methylheptane	58	Ethyl Acetate
24	3-Methylheptane	59	Formaldehyde
25	n-Octane	60	Acetaldehyde
26	n-Nonane	61	Acrolein
27	n-Decane	62	Acetone

Number	Species	Number	Species
28	n-Undecane	63	Propionaldehyde
29	n-Dodecane	64	Butenal
30	Ethylene	65	Butyraldehyde
31	Propene	66	Benzaldehyde
32	1-Butene	67	Isovaleraldehyde
33	cis-2-Butene	68	Valeraldehyde
34	trans-2-Butene	69	Hexaldehyde
35	1-Pentene	70	2-Butanone

Table S3. Performance comparison of initial and optimized fits on VOCs validation set.

Samples ID	Online concentrations (μg/m^3)	Sample-based concentrations (μg/m^3)	Initial fit		Optimized fit	
			Predicted value (μg/m^3)	Relative errors (%)	Predicted value (μg/m^3)	Relative errors (%)
T1	630	927.03	1336.89	44.21	878.09	-5.28
T2	139	242.96	719.76	196.25	239.18	-1.56
T3	8420	12877.57	11127.99	13.59	11795.04	-8.41
T4	2662	4387.86	3890.87	11.33	5016.59	14.33

Table S4. Performance comparison of initial and optimized fits on $PM_{2.5}$ validation set.

Samples ID	Online concentrations (μg/m^3)	Sample-based concentrations (μg/m^3)	Initial fit		Optimized fit	
			Predicted value (μg/m^3)	Relative errors (%)	Predicted value (μg/m^3)	Relative errors (%)
T1	843.75	2167.09	2100.45	-3.08	2246.17	3.65
T2	201.55	399.20	502.85	25.96	386.49	-3.18

Table S5. Confusion matrix for cuisine-type classification, with online-monitored catering enterprises as ground-truth labels and clarified POI-derived categories as predictions.

Ground truth	Predicted						Recall (%)
	CC [a]	SHC [a]	CFF [a]	NCB [a]	OCC [a]	Canteens [a]	
CC	130	3	5	0	10	2	86.67
SHC	0	16	4	0	0	0	80.00
CFF	6	4	42	0	2	0	77.78
NCB	0	0	0	22	1	0	95.65
OCC	5	0	2	0	46	0	86.79
Canteens	5	0	3	0	4	90	88.24
Precision (%)	89.04	69.57	75.00	100	73.02	97.83	

[a] The categories were Cantonese cuisine (CC), Sichuan-Hunan cuisine (SHC), Chinese Fast-Food cuisine (CFF), Non-Chinese cuisine and barbecue (NCB), other Chinese cuisine (OCC) and canteens.

Table S6. The geographical coverage of each domain.

Domains	Geographical coverage
Domain 1	From (98.09°E, 8.44°N) to (134.43°E, 49.58°N)
Domain 2	From (103.72°E, 17.59°N) to (121.24°E, 30.18°N)
Domain 3	From (109.51°E, 20.16°N) to (117.35°E, 25.48°N)

Table S7. Total anthropogenic emissions except for the commercial cooking emissions in Guangdong Province (GD) in d03 domain for year 2023, unit: t/a.

Domain	SO_2	NOx	CO	VOCs	NH_3	PM_{10}	$PM_{2.5}$	BC	OC
GD emissions in d03 domain	195745	1228685	3566864	1258007	461693	732098	292813	27586	83744

Emission inventories for d01 and d02 domains were obtained from the Multi-Resolution Emission Inventory for China (MEIC, http://meicmodel.org). The d03 domain inventory was developed by our research group, excluding commercial cooking emissions in Guangdong Province. Natural emissions for all domains were acquired using the Model of Gases and Aerosols from Nature (MEGAN v3.20). Initial and boundary conditions for inner domains (d02 and d03) were derived from upper-level CMAQ simulation outputs.

Table S8. WRF and CMAQ model configurations.

Model	Parameters	Options
WRF	Land-surface physics scheme	Noah
version 3.9.1	PBL physics scheme	Yenisei University
	Cumulus	Kain-Fritsch cumulus cloud parameterization
	Longwave radiation	Rapid radiative transfer model
	Shortwave radiation	Goddard
	Microphysics	Purdue Lin
CMAQ	Horizontal advection	Yamartino global mass conserving scheme
version 5.4	Horizontal diffusion	Explicit
	Vertical advection	Yamartino global mass conserving scheme
	Vertical diffusion	ACM2
	Gas-phase chemistry	CB06
	Gas-phase chemistry algorithm	EBI
	Aerosol chemistry	AE7
	Dry deposition	M3DRY
	Wet deposition	Accumulation and coarse mode particles completely absorbed in cloud water; Nuclei mode slowly scavenged; Henry's law equilibrium for gases

All domains were vertically divided into 14 layers of varying thicknesses. A five-day spin-up period was implemented to minimize initial condition impacts.

Table S9. Monthly validation of $PM_{2.5}$ prediction using the WRF-CMAQ modeling system at the Tiyuxi and Dinghu (national air quality monitoring stations) of the D3 domain.

Stations/ Region	Months	Mean_obs [a] (μg/m³)	$CASE_{le}$ [b]			$CASE_{UOS}$ [b]			Differential [d]	
			Mean_sim [c] (μg/m³)	R	NMB (%)	Mean_sim [c] (μg/m³)	R	NMB (%)	R [e]	NMB [e] (%)
Guangdong	Annual	21.15	18.38	0.50	-13.10	19.63	0.52	-7.19	0.02↑	5.91↑
Tiyuxi	1	29.83	27.92	0.56	-6.43	30.74	0.61	3.05	0.05↑	3.38↑
	2	33.25	35.36	0.59	6.37	36.21	0.61	8.92	0.02↑	2.56
	3	30.44	29.13	0.58	-4.32	31.81	0.58	4.48	0.00	0.16
	4	24.32	23.24	0.38	-4.45	25.18	0.38	3.55	0.00	0.90↑
	5	23.40	26.16	0.47	11.81	25.59	0.49	9.35	0.02↑	2.46↑
	6	16.77	19.14	0.42	14.16	18.39	0.44	9.70	0.02↑	4.46↑
	7	13.44	15.09	0.52	12.25	14.50	0.56	7.83	0.04↑	4.42↑
	8	16.67	18.97	0.39	13.79	18.59	0.42	11.50	0.03↑	2.29↑
	9	17.94	21.05	0.36	17.32	20.53	0.38	14.43	0.02↑	2.90↑
	10	24.46	28.20	0.62	15.27	27.73	0.62	13.36	0.01↑	1.90↑
	11	32.36	34.57	0.60	6.81	35.08	0.61	8.39	0.01↑	1.59
	12	31.78	30.58	0.62	-3.79	33.23	0.65	4.56	0.03↑	0.78
Dinghu	1	26.60	25.17	0.57	-5.36	25.59	0.57	-3.81	0.00	1.55↑
	2	31.51	29.08	0.48	-7.72	30.23	0.48	-4.06	0.00	3.66↑
	3	28.25	25.63	0.57	-9.25	26.09	0.58	-7.65	0.01↑	1.60↑
	4	23.01	20.35	0.36	-11.58	20.76	0.36	-9.81	0.00	1.77↑
	5	21.61	19.34	0.47	-10.50	19.72	0.48	-8.78	0.01↑	1.72↑
	6	15.51	13.79	0.43	-11.12	14.08	0.43	-9.23	0.00	1.89↑
	7	11.70	10.24	0.37	-12.50	10.46	0.38	-10.60	0.01↑	1.90↑
	8	13.52	11.47	0.34	-15.14	11.77	0.35	-12.93	0.01↑	2.21↑
	9	14.00	11.70	0.35	-16.44	11.93	0.36	-14.75	0.00	1.69↑
	10	18.45	16.25	0.48	-11.93	16.65	0.48	-9.77	0.00	2.17↑
	11	27.19	23.96	0.46	-11.87	24.82	0.47	-8.71	0.01↑	3.16↑
	12	24.26	21.86	0.53	-9.90	22.39	0.54	-7.72	0.01↑	2.18↑

[a] MEAN_obs was monthly average $PM_{2.5}$ observations. [b] $CASE_{UOS}$ and $CASE_{le}$ were the modelling study based on EI_{UOS} and EI_{le} respectively. [c] MEAN_sim was the monthly average $PM_{2.5}$ simulation results. [d] Differential was obtained by subtracting R/NMB in $CASE_{le}$ from R/NMB in $CASE_{UOS}$. [e] The upward arrow indicated that the simulation performance of $CASE_{UOS}$ was improved comparing with that of $CASE_{le}$.

Table S10. Monthly validation of O_3 prediction using the WRF-CMAQ modeling system at the Tiyuxi and Dinghu (national air quality monitoring station) of the D3 domain.

Stations/ Region	Months	Mean_obs [a] (μg/m^3)	$CASE_{le}$ [b]			$CASE_{UOS}$ [b]			Differential [d]	
			Mean_sim [c] (μg/m^3)	R	NMB (%)	Mean_sim [c] (μg/m^3)	R	NMB (%)	R [e]	NMB [e] (%)
Guangdong	Annual	61.01	57.61	0.64	-5.57	57.74	0.64	-4.46	0.00	1.11↑
Tiyuxi	1	47.65	43.97	0.67	-7.73	44.87	0.67	-5.82	0.00	1.91↑
	2	53.81	52.19	0.74	-3.02	53.18	0.75	-1.18	0.01↑	1.83↑
	3	63.83	58.94	0.71	-7.66	59.59	0.71	-6.63	0.00	1.03↑
	4	55.49	49.95	0.61	-9.99	50.76	0.61	-8.53	0.00	1.46↑
	5	66.69	57.17	0.73	-14.27	58.28	0.73	-12.61	0.00	1.66↑
	6	60.18	51.53	0.67	-14.38	52.39	0.67	-12.95	0.00	1.43↑
	7	61.98	53.99	0.73	-12.88	54.57	0.74	-11.96	0.00	0.92↑
	8	62.99	53.72	0.55	-14.73	55.17	0.55	-12.42	0.00	2.31↑
	9	56.00	49.76	0.64	-11.14	50.65	0.64	-9.55	0.00	1.59↑
	10	67.72	59.59	0.62	-12.01	60.64	0.63	-10.45	0.00	1.56↑
	11	63.41	55.77	0.67	-12.05	56.59	0.69	-10.76	0.02↑	1.29↑
	12	40.57	37.62	0.64	-7.27	38.55	0.65	-4.98	0.00	2.29↑
Dinghu	1	50.84	57.98	0.70	14.05	58.01	0.71	14.10	0.01↑	0.05
	2	62.33	67.12	0.76	7.67	66.45	0.76	6.60	0.00	1.07↑
	3	73.89	76.89	0.68	4.06	76.26	0.68	3.22	0.00	0.84↑
	4	52.99	57.71	0.58	8.92	57.24	0.58	8.02	0.01↑	0.89↑
	5	68.77	63.84	0.62	-7.17	64.58	0.63	-6.10	0.00	1.07↑
	6	63.66	62.34	0.69	-2.08	63.00	0.69	-1.03	0.00	1.04↑
	7	55.68	59.19	0.74	6.30	58.45	0.75	4.97	0.01↑	1.33↑
	8	63.08	68.57	0.66	8.70	67.74	0.68	7.38	0.01↑	1.32↑
	9	59.51	66.06	0.80	11.01	65.59	0.80	10.21	0.00	0.80↑
	10	68.71	76.29	0.66	11.03	76.35	0.67	11.13	0.01↑	0.10
	11	72.95	78.81	0.71	8.02	79.01	0.71	8.30	0.00	0.28
	12	51.71	58.80	0.64	13.71	58.88	0.65	13.85	0.01↑	0.14

[a] MEAN_obs was monthly average $PM_{2.5}$ observations. [b] $CASE_{UOS}$ and $CASE_{le}$ were the modelling study based on EI_{UOS} and EI_{le} respectively. [c] MEAN_sim was the monthly average $PM_{2.5}$ simulation results. [d] Differential was obtained by subtracting R/NMB in $CASE_{le}$ from R/NMB in $CASE_{UOS}$. [e] The upward arrow indicated that the simulation performance of $CASE_{UOS}$ was improved comparing with that of $CASE_{le}$

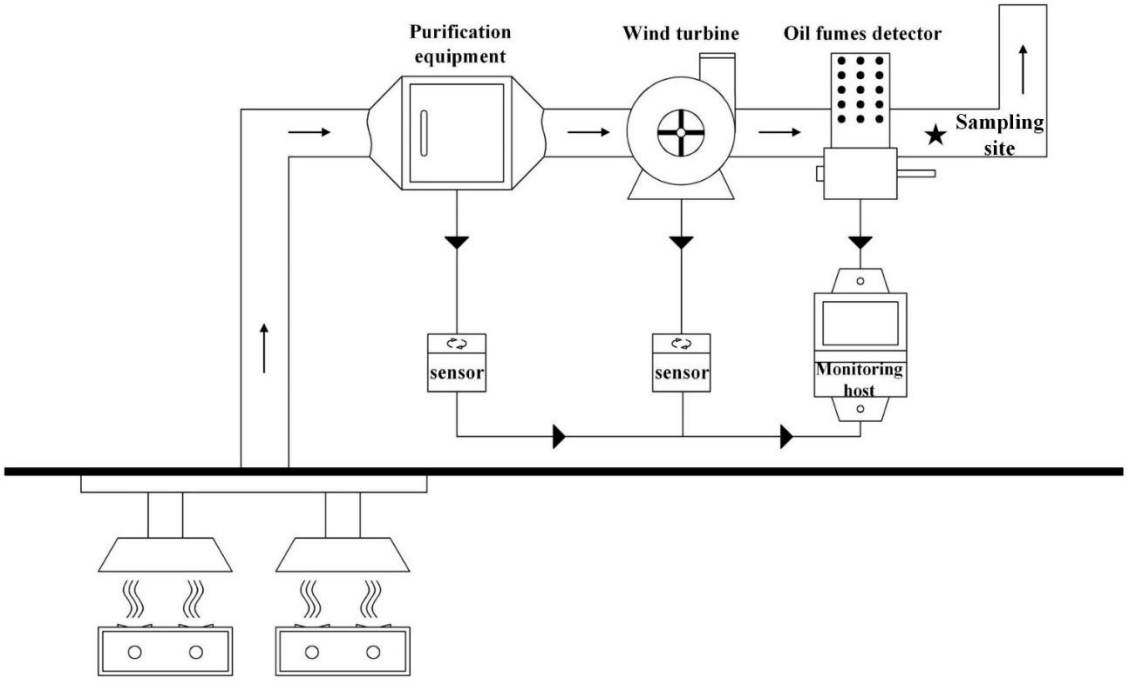

Fig. S1. The structure of the online oil fumes monitoring system. The black five-pointed star represented the sampling sites.

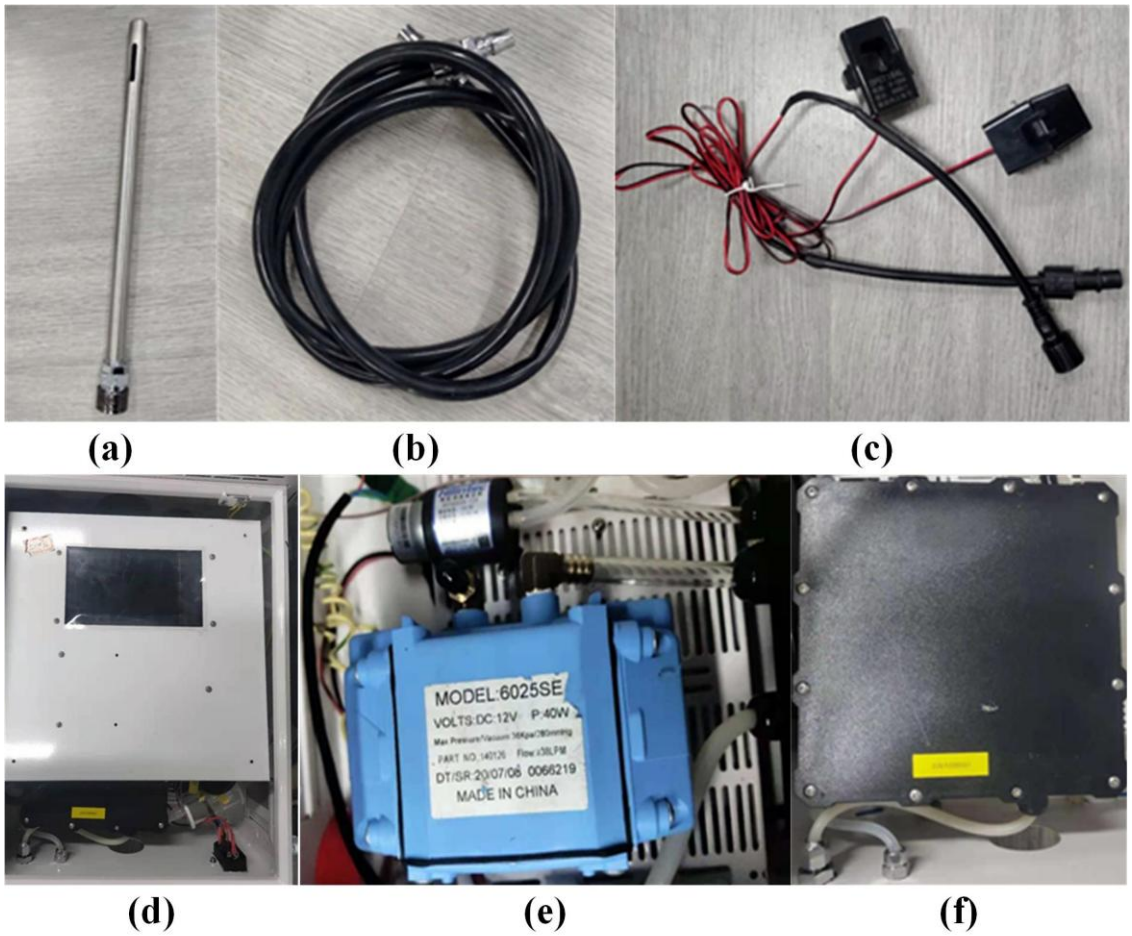

Fig. S2. Hardware of online oil fumes monitoring system. (a) Oil fumes detector; (b) Pitot tube; (c) sensors installed in purification equipment and wind turbines; (d) monitoring host; (e) pump; (f) gas analysis module.

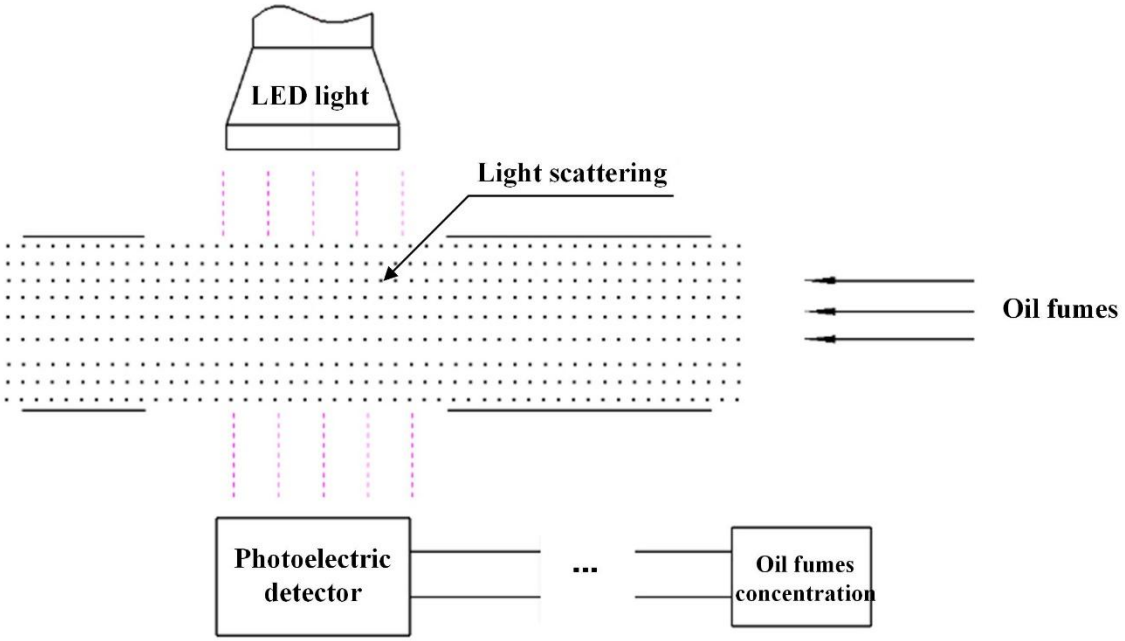

Fig. S3. The operation principle of the laser scattering technology for PM2.5 concentration quantification in the oil fumes.

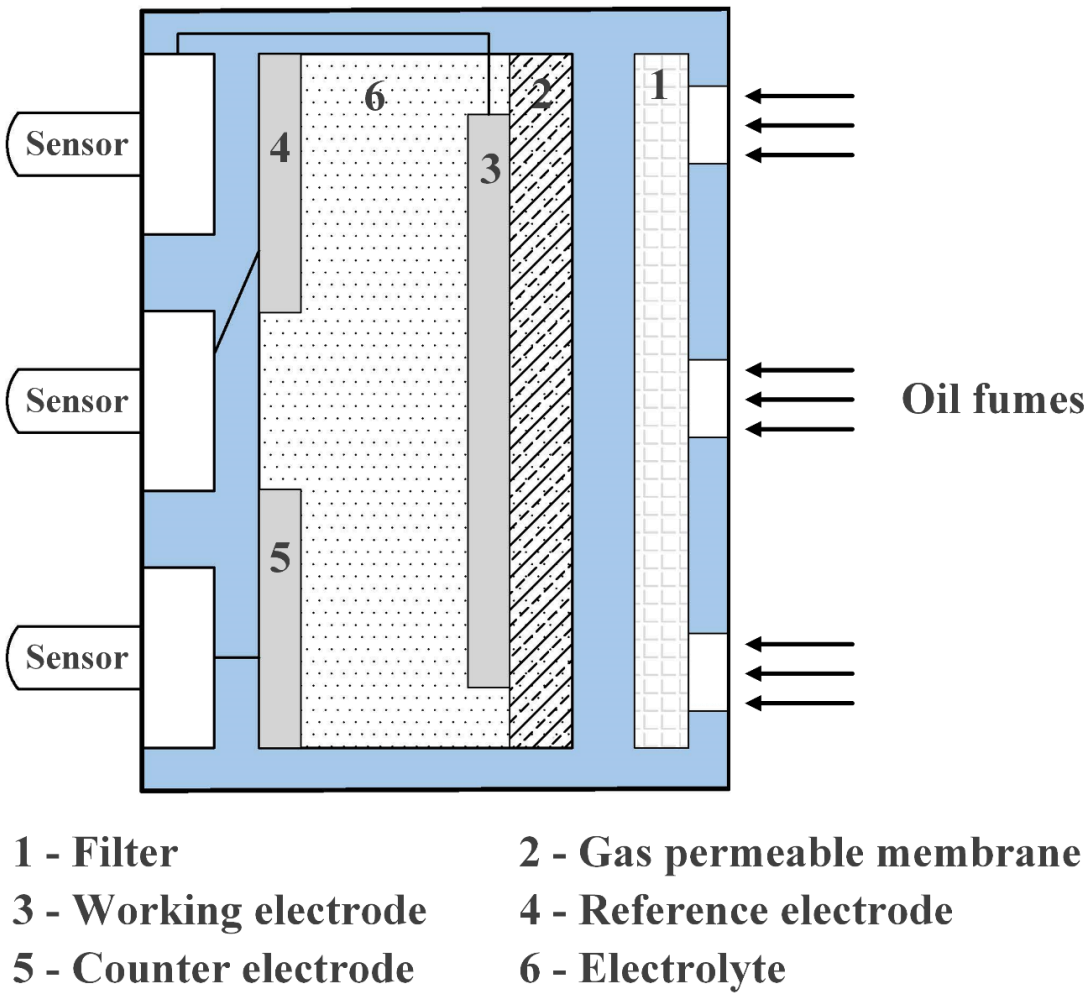

Fig. S4. The operation principle of the electrochemical detection technology for non-methane VOCs (VOCs) concentration quantification in the oil fumes.

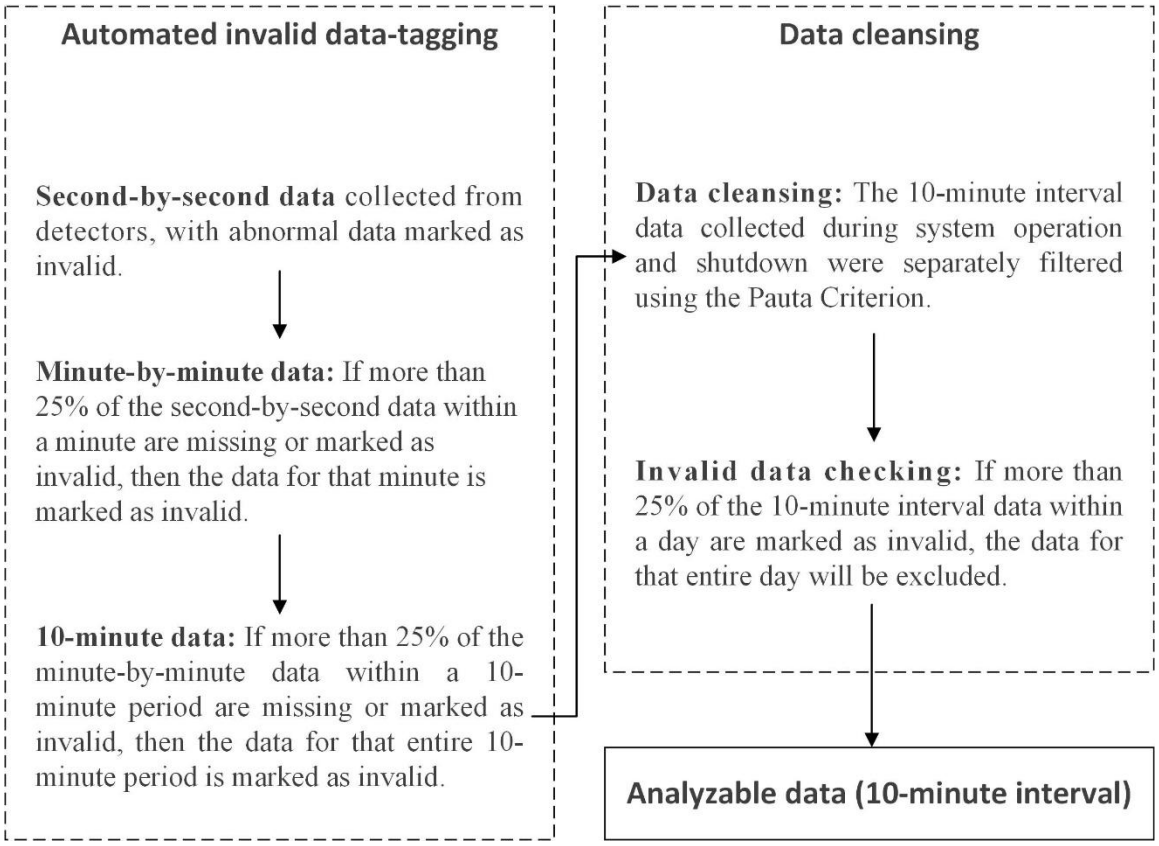

Fig. S5. The workflow for online oil fumes data cleansing.

First, data detected during system shutdowns were systematically excluded based on system status flags. Second, temporally stratified OOFM data groups were generated by aligning 10-minute temporal labels across monitoring days, followed by application of the Pauta criterion (3σ principle) to eliminate values exceeding the μ±3σ statistical boundaries within each chronologically matched subset.

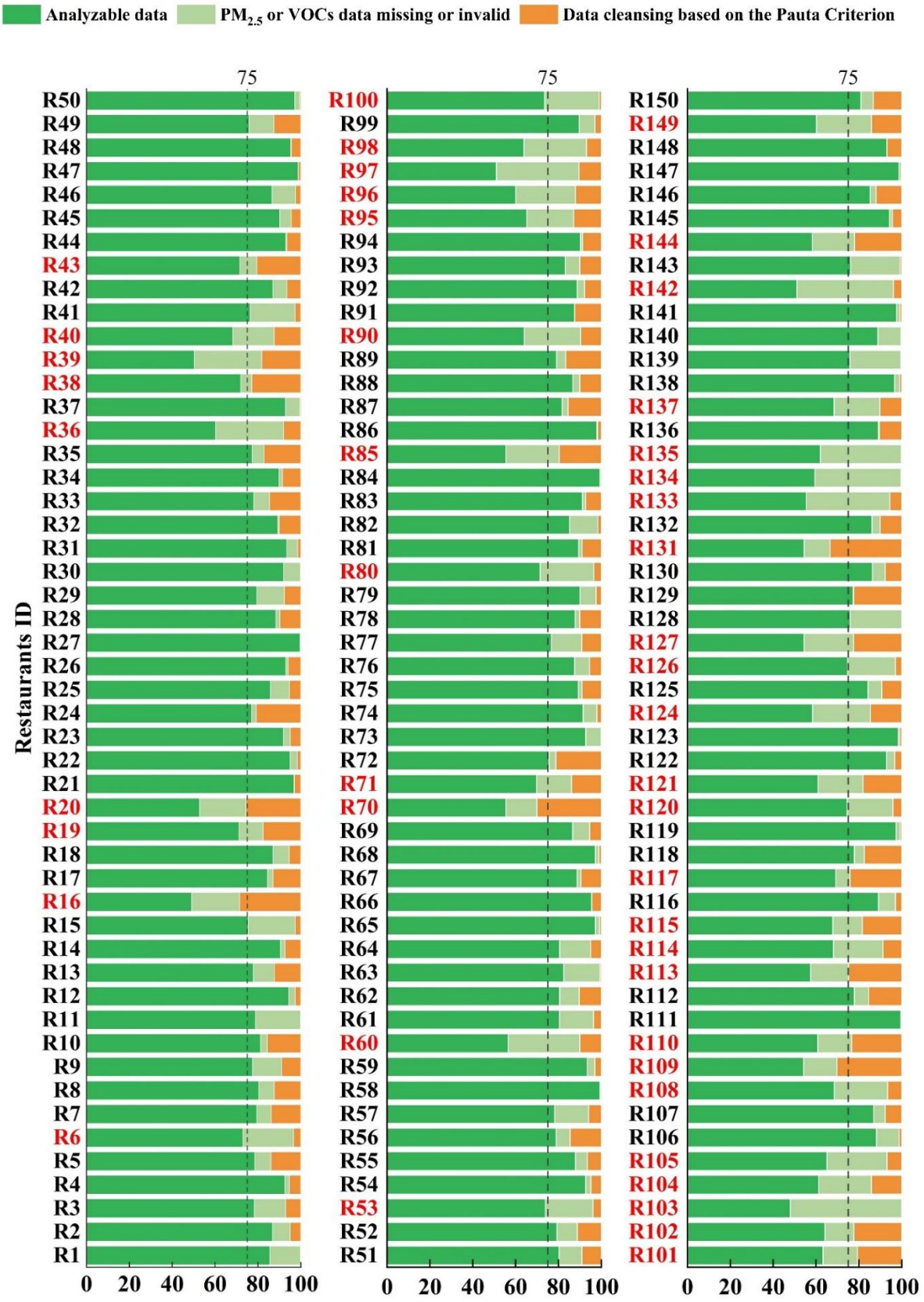
Analyzable data
PM2.5 or VOCs data missing or invalid
Data cleansing based on the Pauta Criterion
Restaurants ID
75
75
75
R50 R49 R48 R47 R46 R45 R44 R43 R42 R41 R40 R39 R38 R37 R36 R35 R34 R33 R32 R31 R30 R29 R28 R27 R26 R25 R24 R23 R22 R21 R20 R19 R18 R17 R16 R15 R14 R13 R12 R11 R10 R9 R8 R7 R6 R5 R4 R3 R2 R1
R100 R99 R98 R97 R96 R95 R94 R93 R92 R91 R90 R89 R88 R87 R86 R85 R84 R83 R82 R81 R80 R79 R78 R77 R76 R75 R74 R73 R72 R71 R70 R69 R68 R67 R66 R65 R64 R63 R62 R61 R60 R59 R58 R57 R56 R55 R54 R53 R52 R51
R150 R149 R148 R147 R146 R145 R144 R143 R142 R141 R140 R139 R138 R137 R136 R135 R134 R133 R132 R131 R130 R129 R128 R127 R126 R125 R124 R123 R122 R121 R120 R119 R118 R117 R116 R115 R114 R113 R112 R111 R110 R109 R108 R107 R106 R105 R104 R103 R102 R101
0 20 40 60 80 100
0 20 40 60 80 100
0 20 40 60 80 100

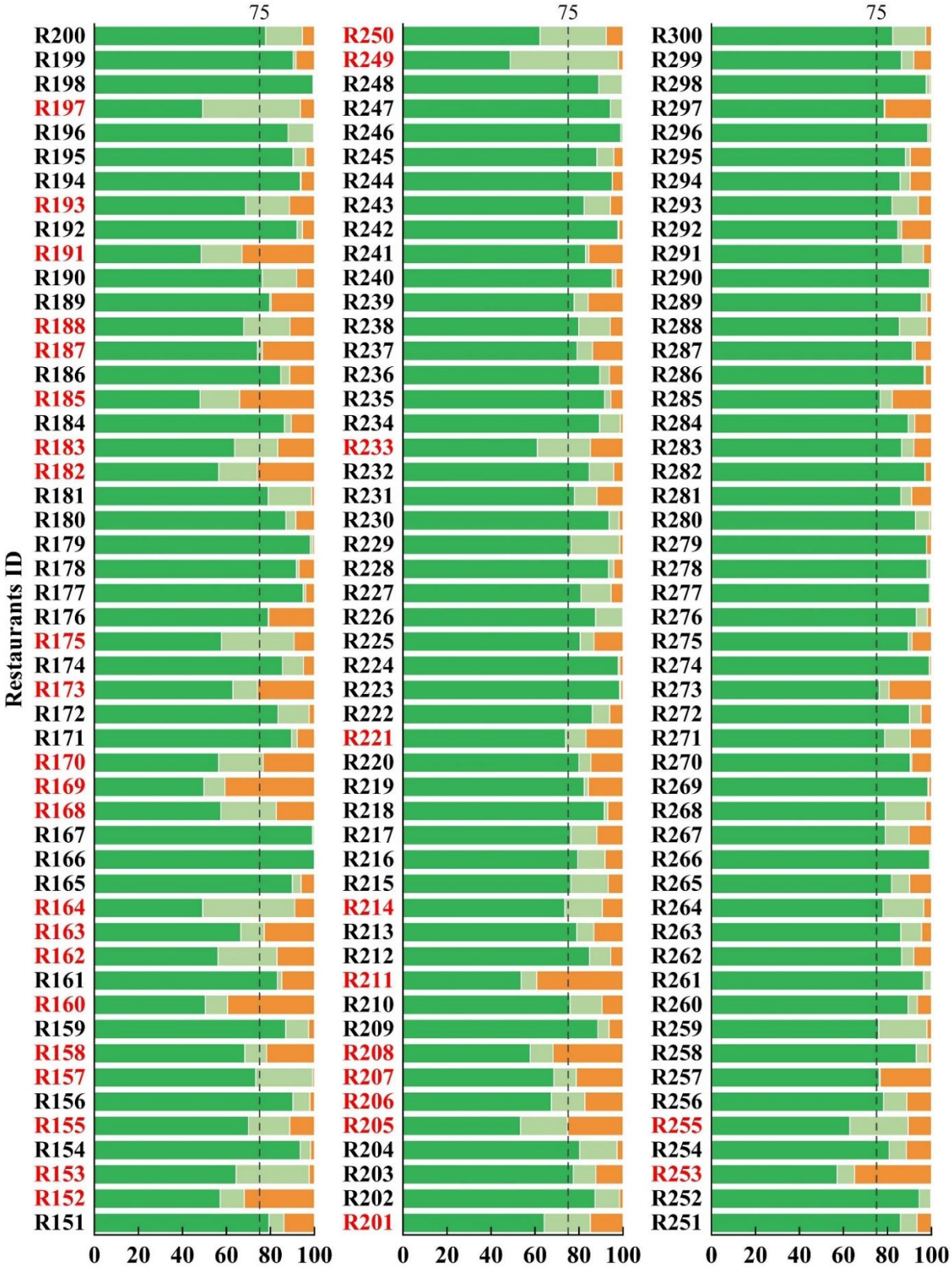
Restaurants ID
75
75
75
R200
R199
R198
R197
R196
R195
R194
R193
R192
R191
R190
R189
R188
R187
R186
R185
R184
R183
R182
R181
R180
R179
R178
R177
R176
R175
R174
R173
R172
R171
R170
R169
R168
R167
R166
R165
R164
R163
R162
R161
R160
R159
R158
R157
R156
R155
R154
R153
R152
R151
R250
R249
R248
R247
R246
R245
R244
R243
R242
R241
R240
R239
R238
R237
R236
R235
R234
R233
R232
R231
R230
R229
R228
R227
R226
R225
R224
R223
R222
R221
R220
R219
R218
R217
R216
R215
R214
R213
R212
R211
R210
R209
R208
R207
R206
R205
R204
R203
R202
R201
R300
R299
R298
R297
R296
R295
R294
R293
R292
R291
R290
R289
R288
R287
R286
R285
R284
R283
R282
R281
R280
R279
R278
R277
R276
R275
R274
R273
R272
R271
R270
R269
R268
R267
R266
R265
R264
R263
R262
R261
R260
R259
R258
R257
R256
R255
R254
R253
R252
R251
0 20 40 60 80 100
0 20 40 60 80 100
0 20 40 60 80 100

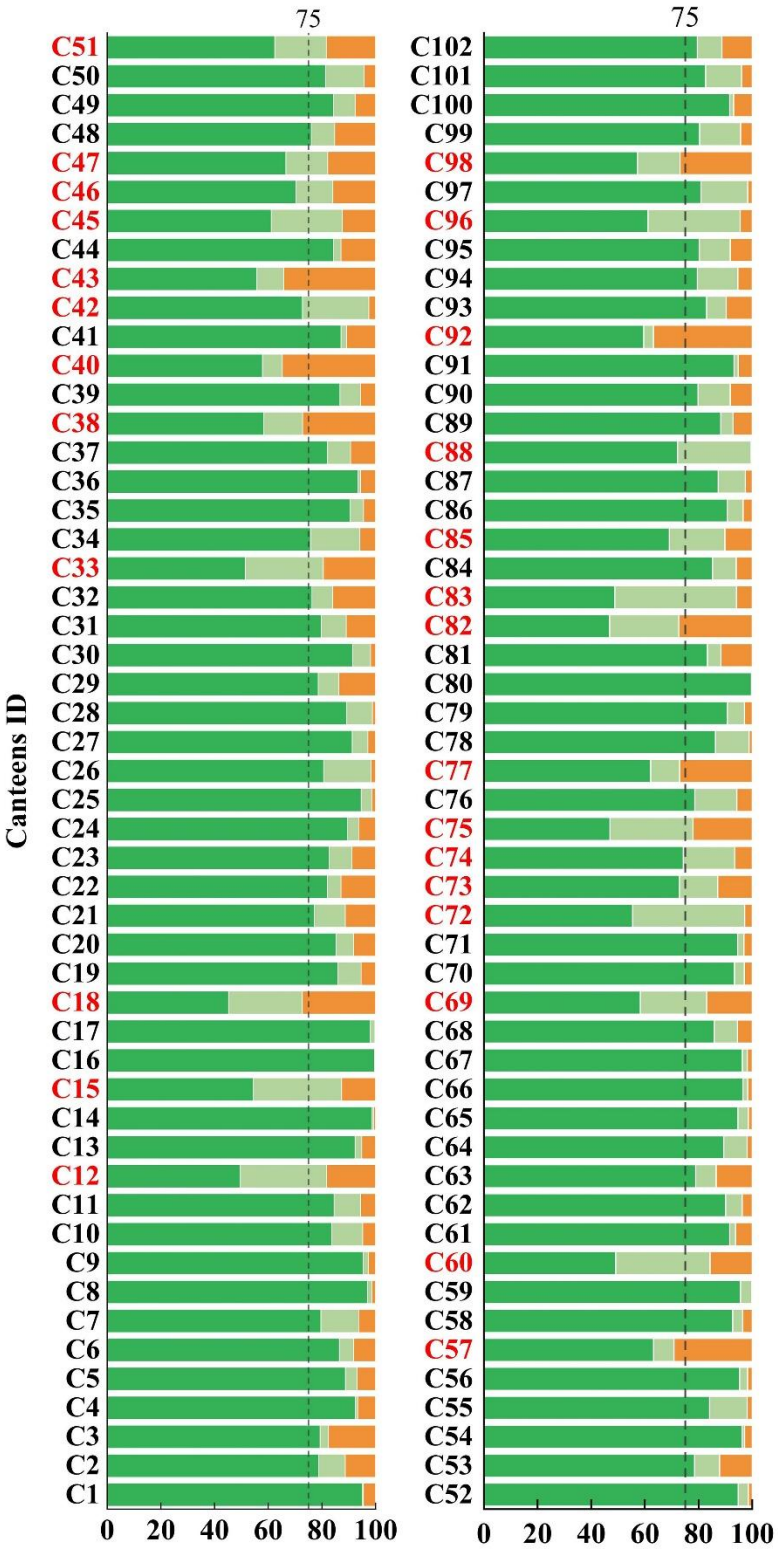

Fig. S6. The validity rates of the post-processing OOFM data for total 251 restaurants and 102 canteens

Fig. S7. The preconcentrator coupled with a Gas Chromatograph/Mass Selective Detector/Flame Ionization Detector/Electron Capture Detector (GC-MSD/FID/ECD)

Fig. S8. The High-Performance Liquid Chromatography (HPLC) system.

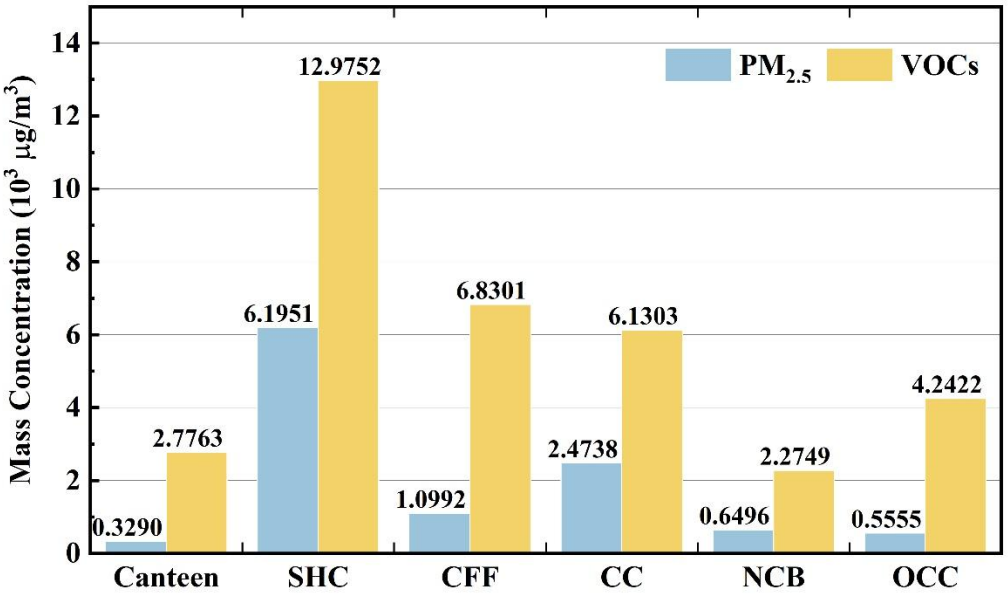

Fig. S9. Mean concentrations of PM2.5 and VOCs in emission samples from six cuisines, including Cantonese cuisine (CC), Sichuan-Hunan cuisine (SHC), Chinese Fast-Food cuisine (CFF), Non-Chinese cuisine and barbecue (NCB), other Chinese cuisine (OCC), and institutional canteens.

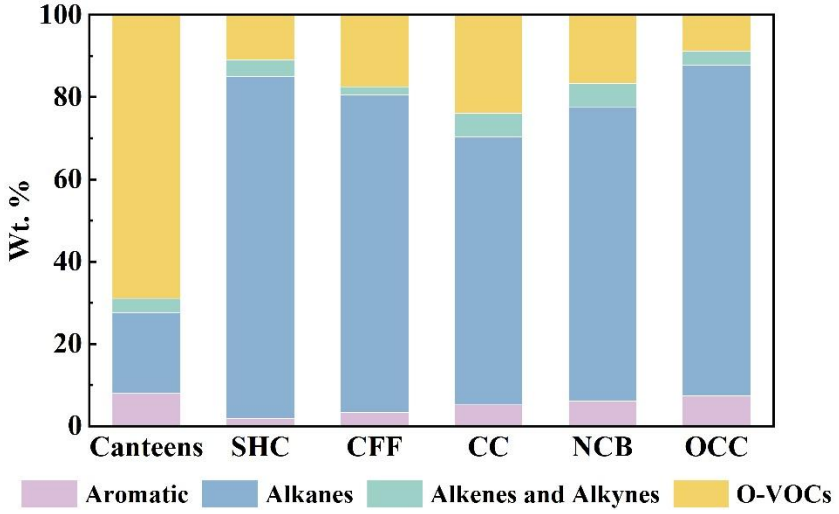

Fig. S10. Mass fractions (wt.%) of VOCs compounds in emissions from the six cuisine types, including Cantonese cuisine (CC), Sichuan-Hunan cuisine (SHC), Chinese fast-food (CFF), Non-Chinese cuisine and barbecue (NCB), other Chinese cuisine (OCC) and institutional canteens.

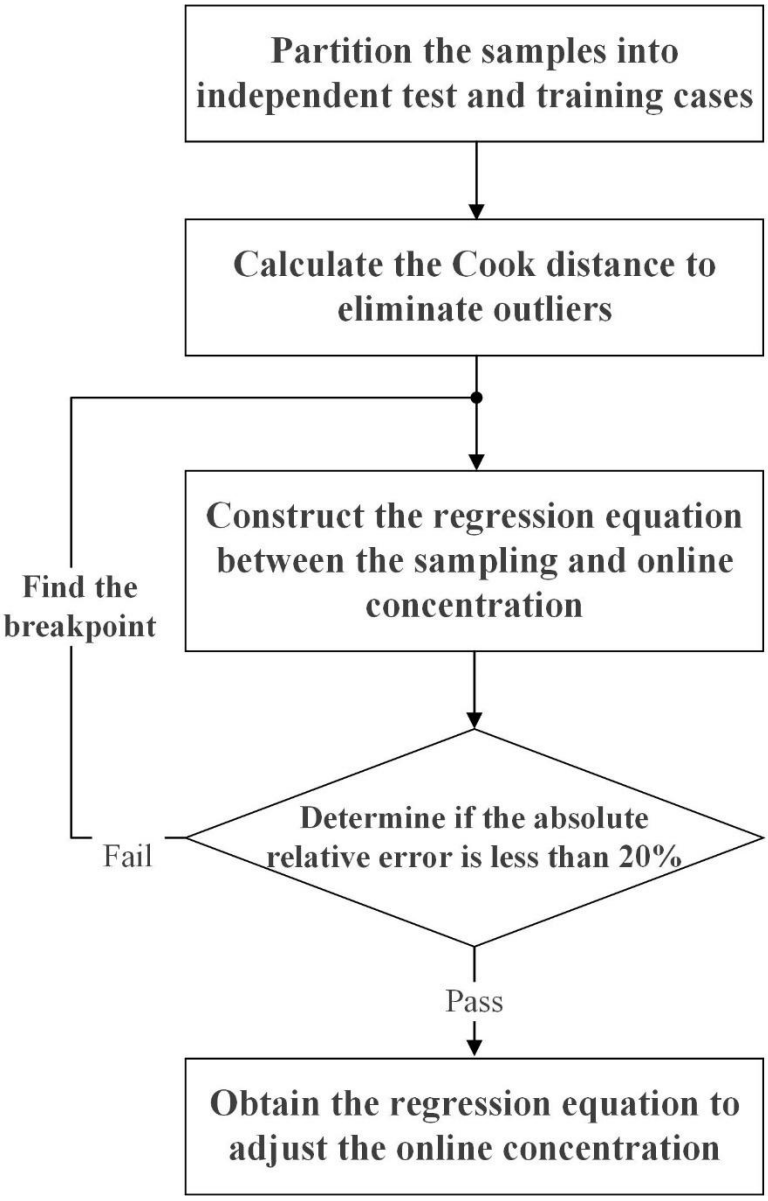

Fig. S11. The workflow for establishing a functional relationship between the OOFM data and the sampled concentrations for the OOFM data calibration.

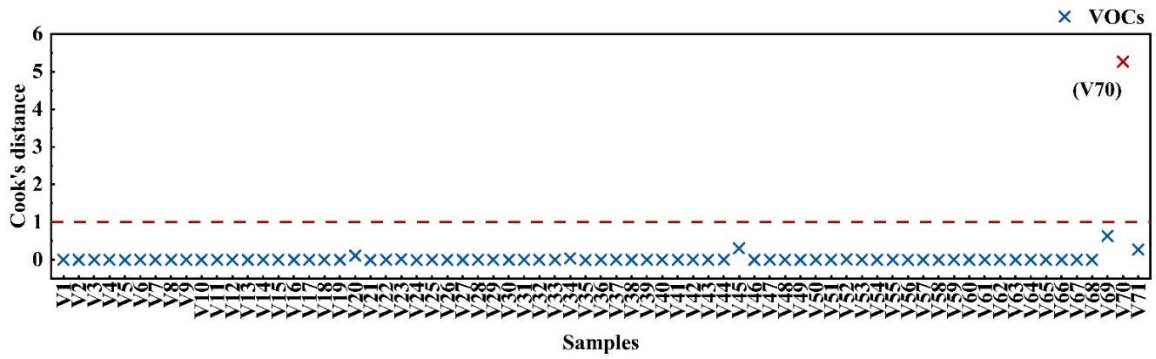

Fig. S12. The Cook's distance for the VOCs samples.

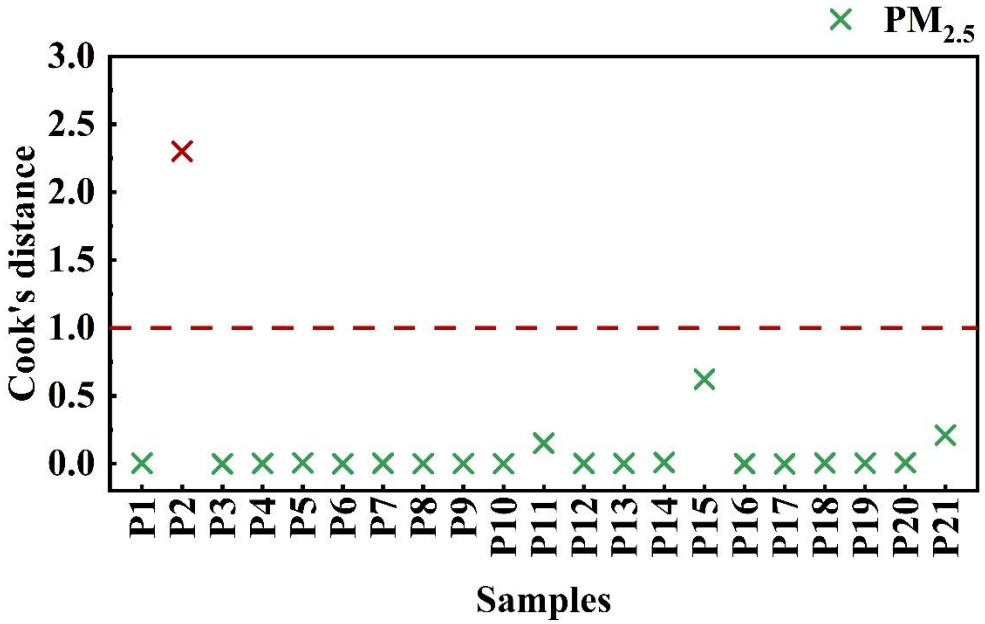

Fig. S13. The Cook's distance for the PM2.5 samples.

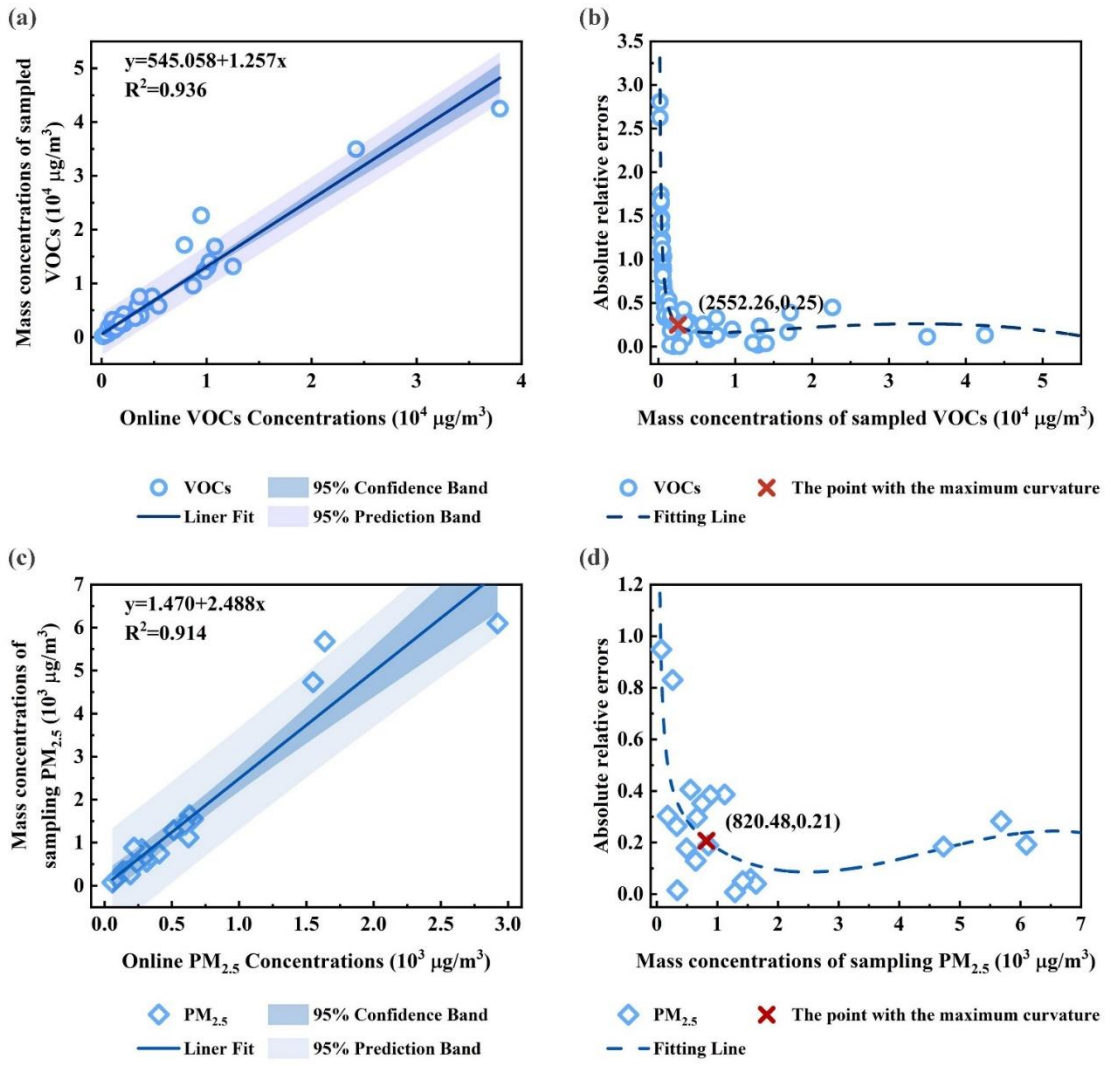

Fig. S14. (a) Scatter plot of sample-based versus online-monitored VOCs concentration with fitted calibration curve which was derived for the calibration of online monitoring VOCs concentration. (b) Scatter plot of calibration residuals (from a) versus sample-based VOCs concentration (blue circles) with fitted curve. The inflection point (red cross), identified by curve derivation, defines the breakpoint for partitioning the calibration in (a). (c) Scatter plot of sample-based versus online-monitored PM2.5 concentration with fitted calibration curve which was derived for the calibration of online monitoring PM2.5 concentration. (d) Scatter plot of calibration residuals (from c) versus sample-based PM2.5 concentration (blue rhombuses) with fitted curve. The inflection point (red cross), identified by curve derivation, defines the breakpoint for partitioning the calibration in (c).

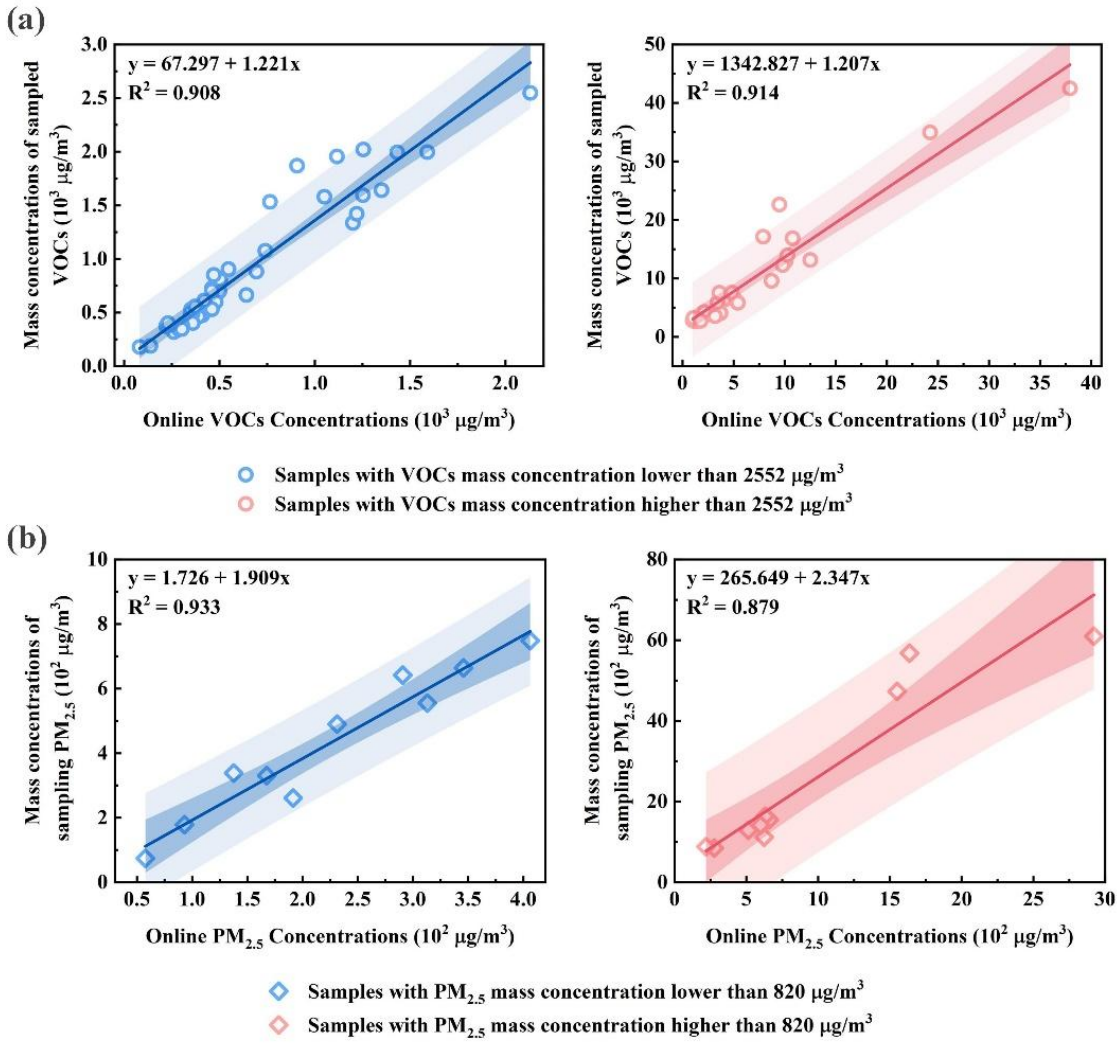

Fig. S15. (a) Scatter plot of sample-based versus online-monitored VOCs concentration with piecewise fitted calibration curve which was derived for the calibration of online monitoring VOCs concentration. (b) Scatter plot of sample-based versus online-monitored PM2.5 concentration with piecewise fitted calibration curve which was derived for the calibration of online monitoring PM2.5 concentration.

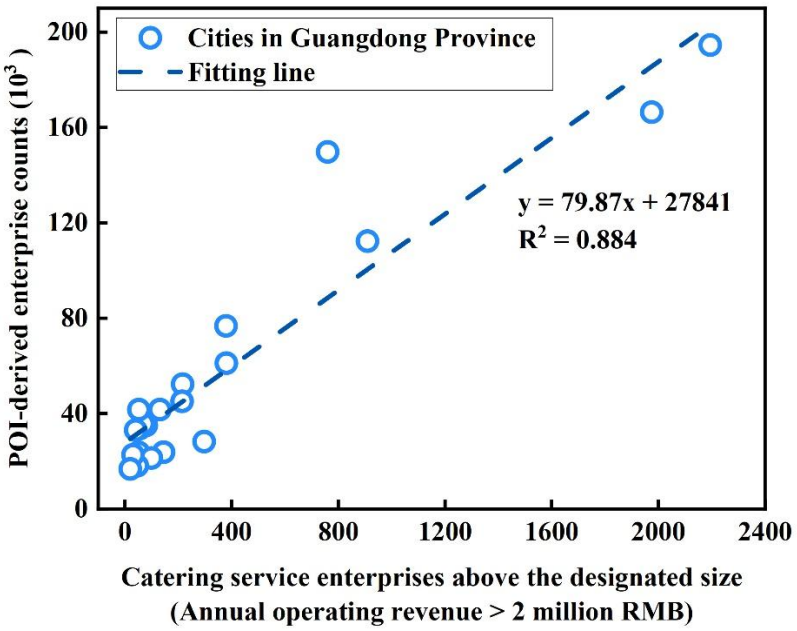

Fig. S16. City-level linear regression between clarified POI-derived catering establishment counts and yearbook-reported above-designated-size catering service enterprises (ADSEs)

As POI data quality may impact emission inventory estimates through both the total number of catering establishments and their classification, we evaluated the compiled POI dataset using external validation against official statistics for catering service enterprises above designated size (ADSEs; annual operating revenue over 2 million RMB) and the dataset of online-monitored catering enterprises (OOFM dataset). Regarding the performance of POI-derived establishment counts, we conducted a city-level regression analysis comparing the number of catering POIs with the yearbook-reported ADSEs. The regression yielded an R^2 of 0.884, showing that POI counts scale systematically with yearbook-reported ADSE counts across cities, thus exhibiting strong concordance between the two city-level totals. Moreover, all catering enterprises with online monitoring were successfully matched to the corresponding POI entries, suggesting that the POI dataset provides sufficient coverage of actual catering establishments.

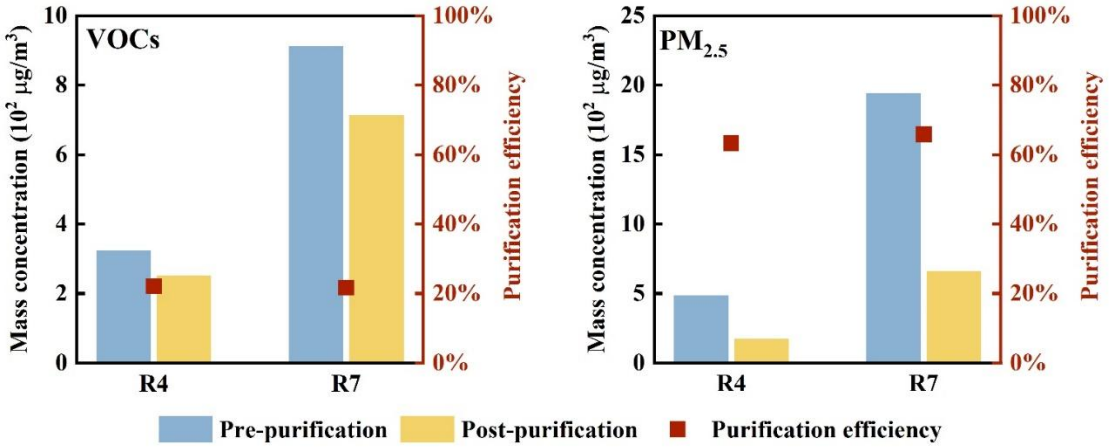

Fig. S17. The mass concentrations (μg/m3) of VOCs and PM2.5, along with the corresponding purification efficiency (%), for two selected restaurants. The left y-axis shows the average concentrations of sampled VOCs and PM2.5 emissions before and after purification equipment, while the right y-axis indicates the calculated purification efficiency based on these concentrations for these two restaurants.

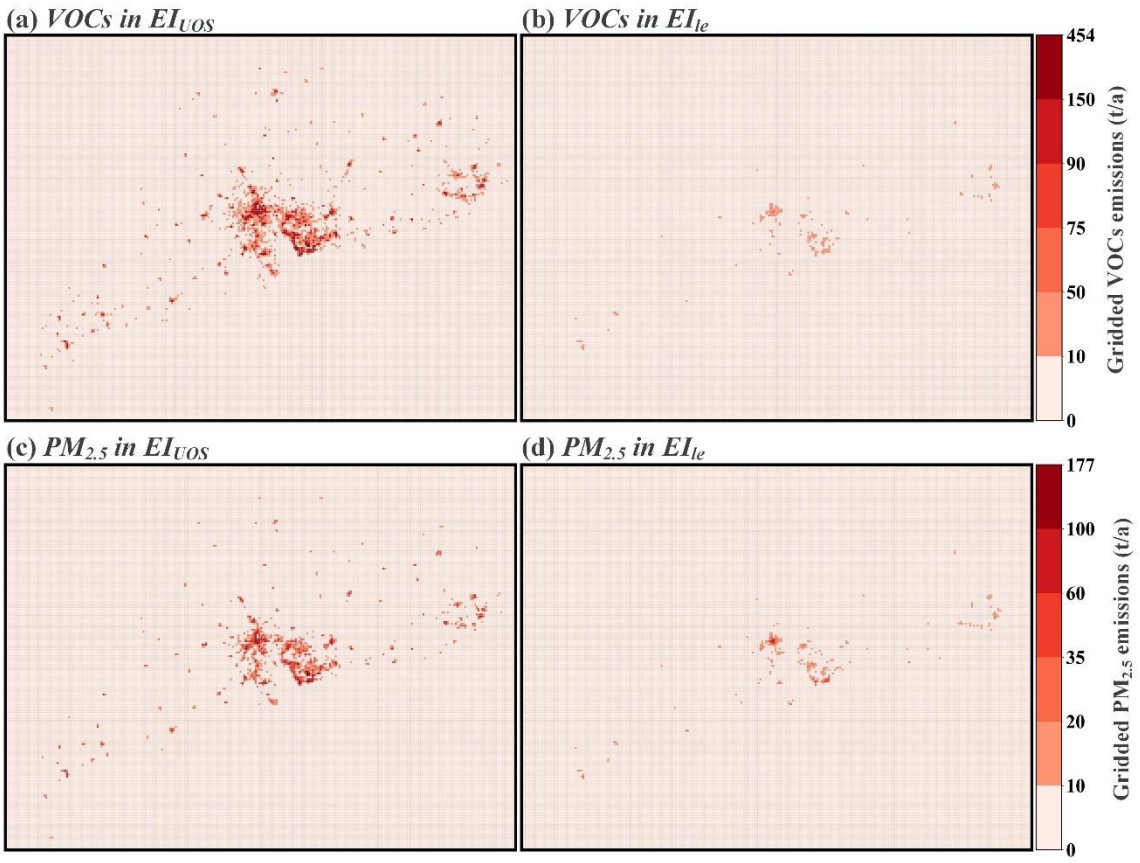

Fig. S18. Gridded VOCs (a, b) and $PM_{2.5}$ (c, d) emissions from commercial cooking in Guangdong Province in 2023, based on EIUOS and EIle emission inventories.

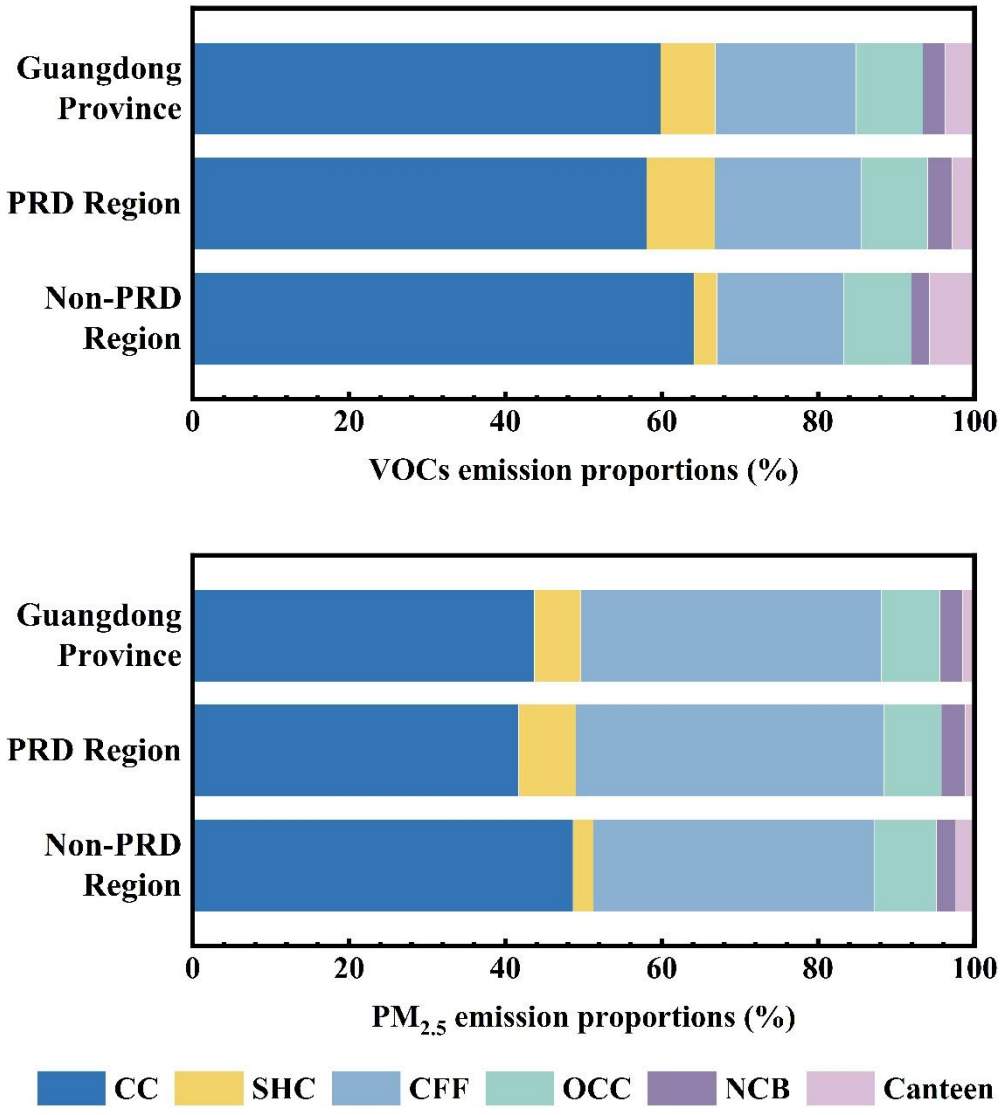

Fig. S19. The proportion of VOCs and $PM_{2.5}$ emissions from individual cuisine types relative to the total commercial cooking emissions in Guangdong Province under EI_{UOS}.

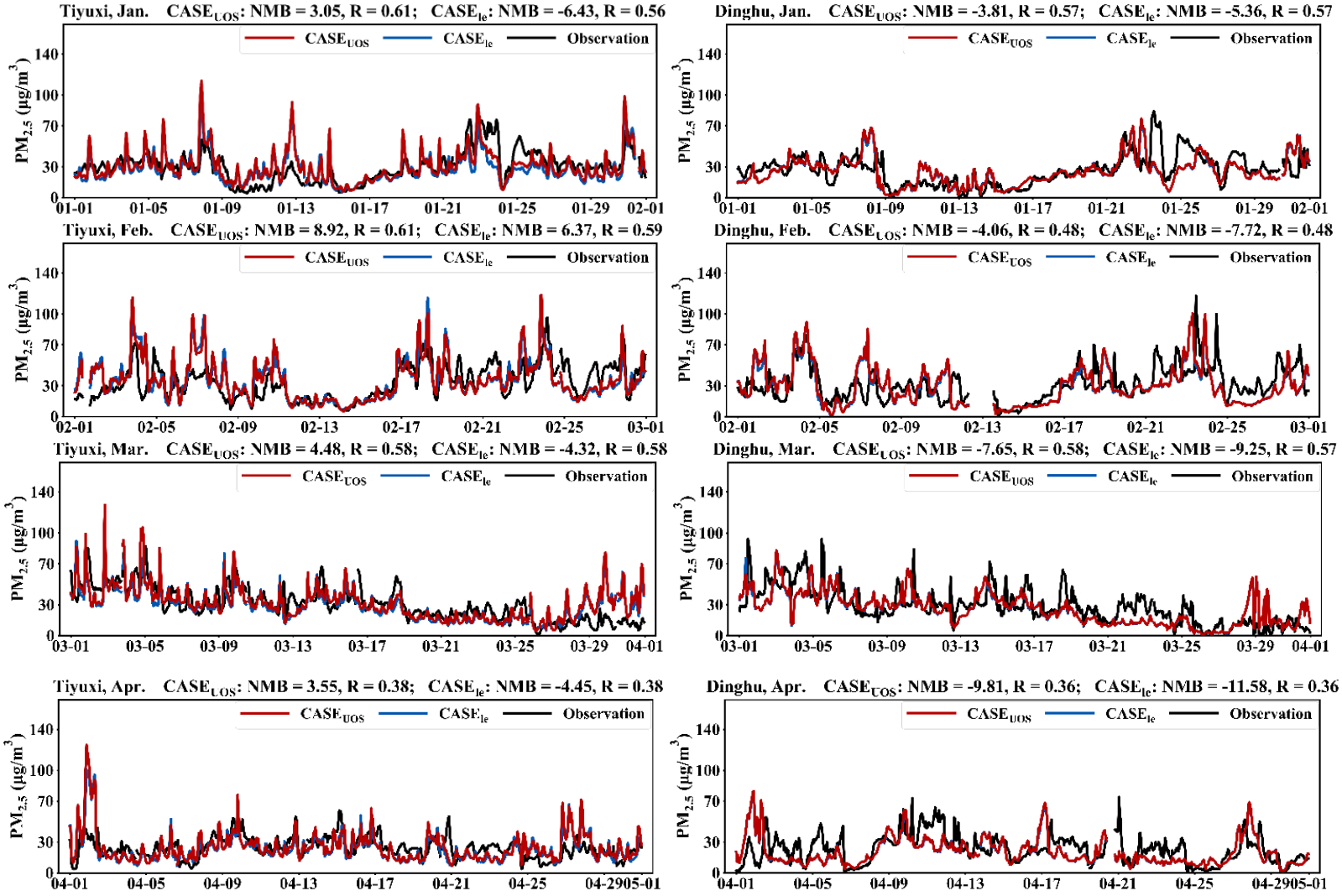
Tiyuxi, Jan. CASE$_{UOS}$: NMB = 3.05, R = 0.61; CASE$_{le}$: NMB = -6.43, R = 0.56
Dinghu, Jan. CASE$_{UOS}$: NMB = -3.81, R = 0.57; CASE$_{le}$: NMB = -5.36, R = 0.57
Tiyuxi, Feb. CASE$_{UOS}$: NMB = 8.92, R = 0.61; CASE$_{le}$: NMB = 6.37, R = 0.59
Dinghu, Feb. CASE$_{UOS}$: NMB = -4.06, R = 0.48; CASE$_{le}$: NMB = -7.72, R = 0.48
Tiyuxi, Mar. CASE$_{UOS}$: NMB = 4.48, R = 0.58; CASE$_{le}$: NMB = -4.32, R = 0.58
Dinghu, Mar. CASE$_{UOS}$: NMB = -7.65, R = 0.58; CASE$_{le}$: NMB = -9.25, R = 0.57
Tiyuxi, Apr. CASE$_{UOS}$: NMB = 3.55, R = 0.38; CASE$_{le}$: NMB = -4.45, R = 0.38
Dinghu, Apr. CASE$_{UOS}$: NMB = -9.81, R = 0.36; CASE$_{le}$: NMB = -11.58, R = 0.36
CASE$_{UOS}$
CASE$_{le}$
Observation
PM$_{2.5}$ (μg/m^3)
0
30
70
100
140
01-01 01-05 01-09 01-13 01-17 01-21 01-25 01-29 02-01
02-01 02-05 02-09 02-13 02-17 02-21 02-25 03-01
03-01 03-05 03-09 03-13 03-17 03-21 03-25 03-29 04-01
04-01 04-05 04-09 04-13 04-17 04-21 04-25 04-29 05-01

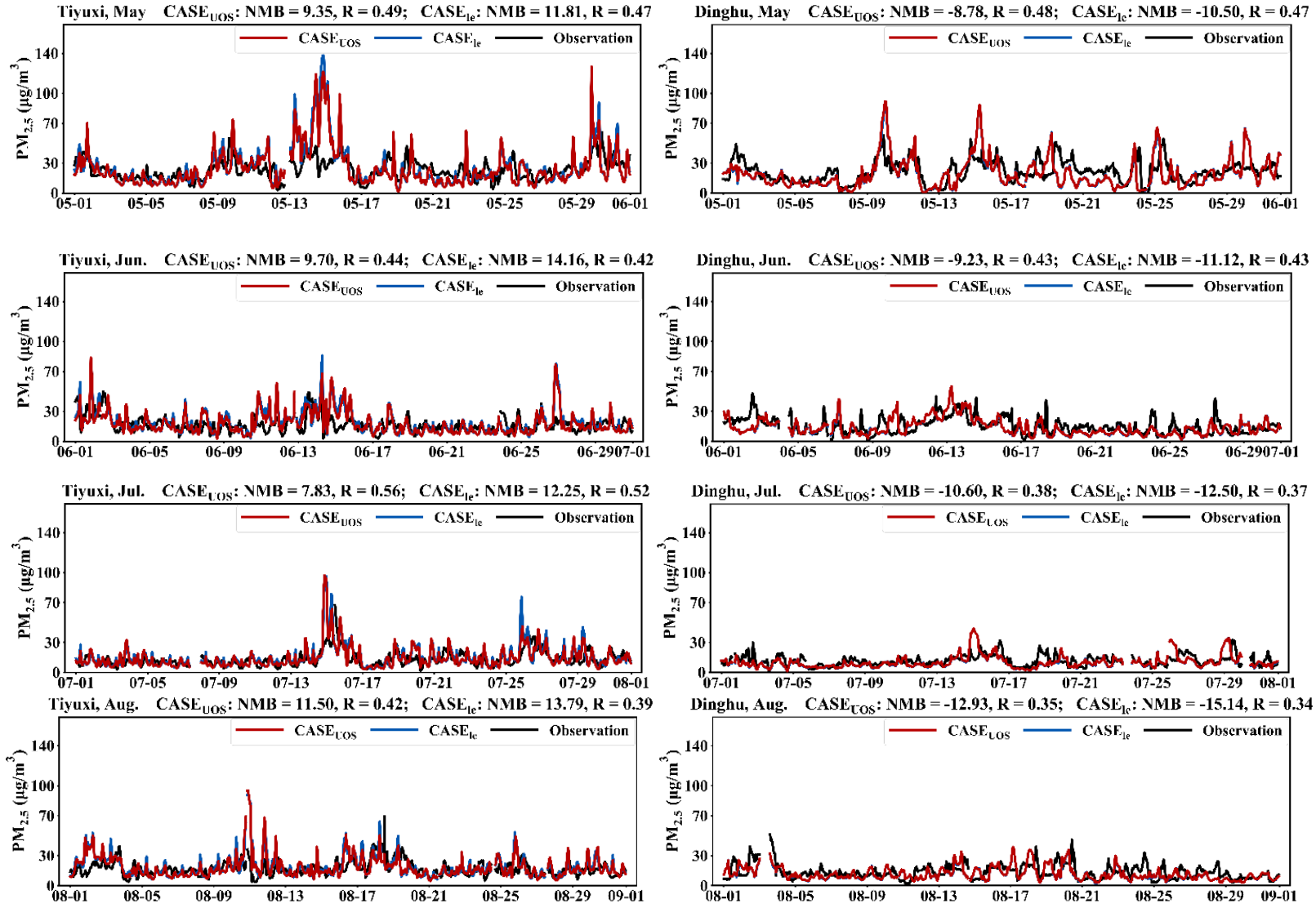
Tiyuxi, May CASE$_{UOS}$: NMB = 9.35, R = 0.49; CASE$_{le}$: NMB = 11.81, R = 0.47
Dinghu, May CASE$_{UOS}$: NMB = -8.78, R = 0.48; CASE$_{le}$: NMB = -10.50, R = 0.47
Tiyuxi, Jun. CASE$_{UOS}$: NMB = 9.70, R = 0.44; CASE$_{le}$: NMB = 14.16, R = 0.42
Dinghu, Jun. CASE$_{UOS}$: NMB = -9.23, R = 0.43; CASE$_{le}$: NMB = -11.12, R = 0.43
Tiyuxi, Jul. CASE$_{UOS}$: NMB = 7.83, R = 0.56; CASE$_{le}$: NMB = 12.25, R = 0.52
Dinghu, Jul. CASE$_{UOS}$: NMB = -10.60, R = 0.38; CASE$_{le}$: NMB = -12.50, R = 0.37
Tiyuxi, Aug. CASE$_{UOS}$: NMB = 11.50, R = 0.42; CASE$_{le}$: NMB = 13.79, R = 0.39
Dinghu, Aug. CASE$_{UOS}$: NMB = -12.93, R = 0.35; CASE$_{le}$: NMB = -15.14, R = 0.34
CASE$_{UOS}$
CASE$_{le}$
Observation
PM$_{2.5}$ (μg/m^3)
0
30
70
100
140
05-01 05-05 05-09 05-13 05-17 05-21 05-25 05-29 06-01
06-01 06-05 06-09 06-13 06-17 06-21 06-25 06-29 07-01
07-01 07-05 07-09 07-13 07-17 07-21 07-25 07-29 08-01
08-01 08-05 08-09 08-13 08-17 08-21 08-25 08-29 09-01

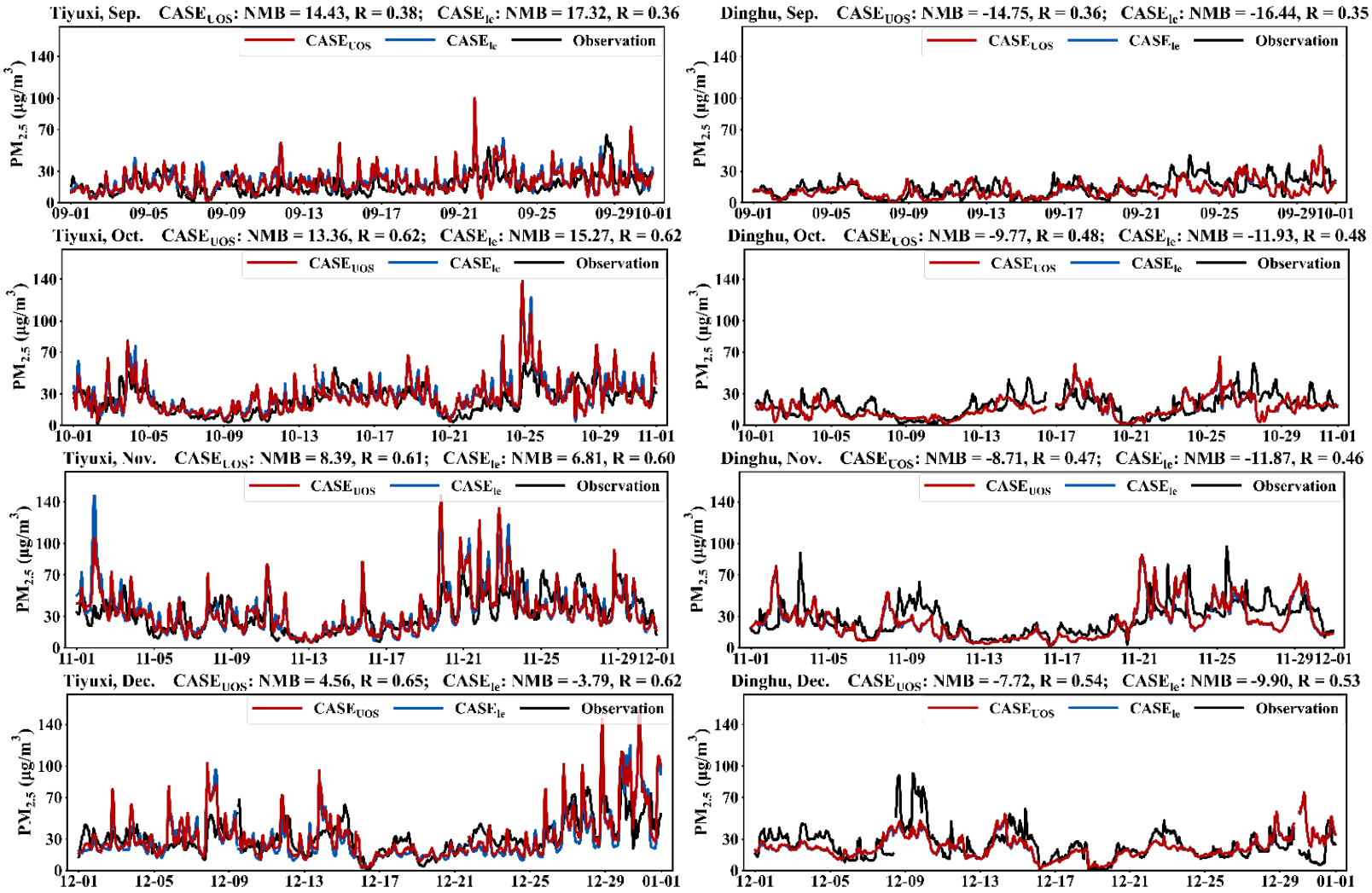

Fig. S20. Comparison of the observed and simulated hourly $PM_{2.5}$ time series from $CASE_{le}$ and $CASE_{UOS}$ for each month in 2023 at Tiyuxi (left) and Dinghu (right), respectively.

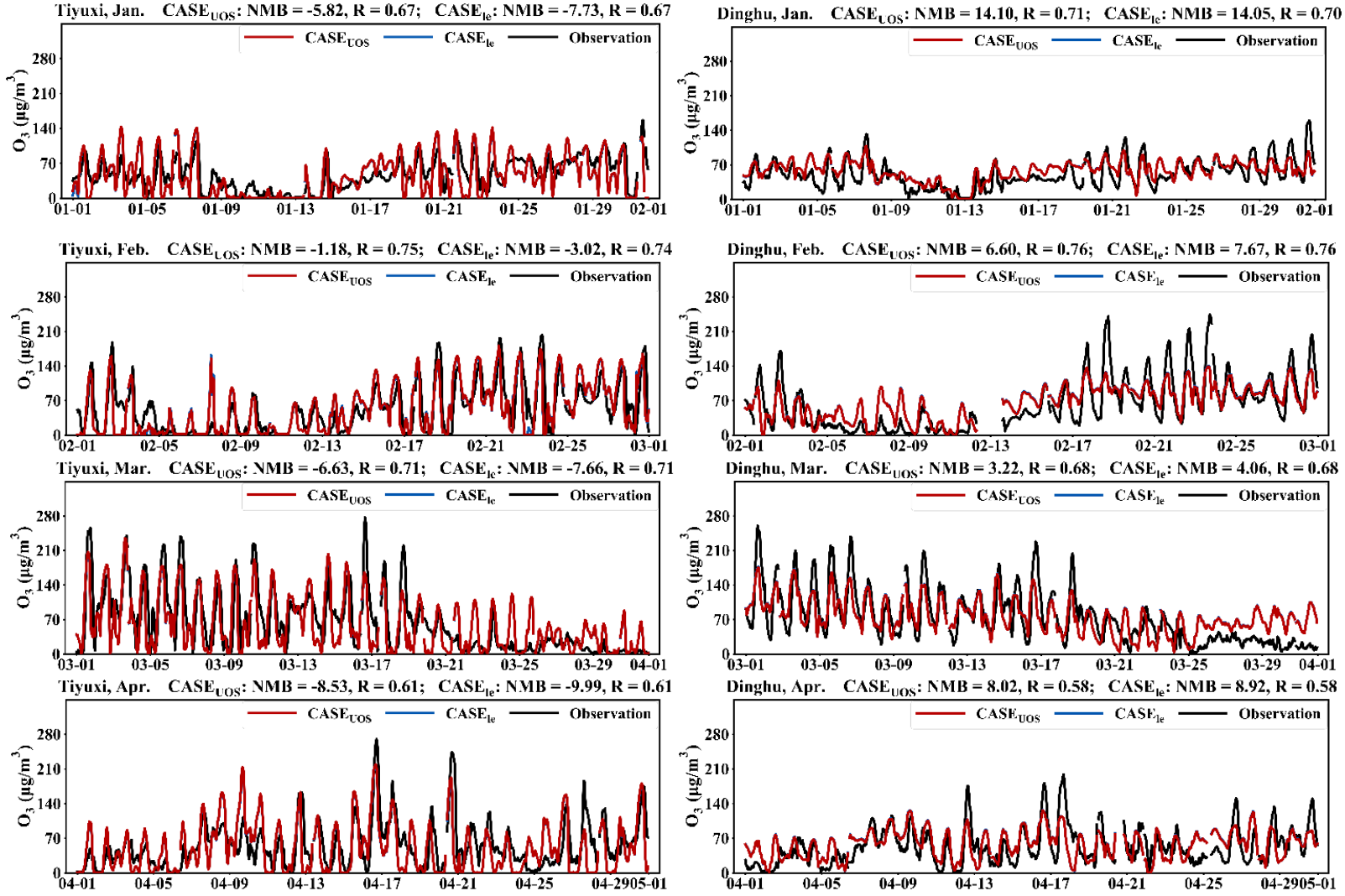
Tiyuxi, Jan. CASE$_{UOS}$: NMB = -5.82, R = 0.67; CASE$_{Ie}$: NMB = -7.73, R = 0.67
Dinghu, Jan. CASE$_{UOS}$: NMB = 14.10, R = 0.71; CASE$_{Ie}$: NMB = 14.05, R = 0.70
Tiyuxi, Feb. CASE$_{UOS}$: NMB = -1.18, R = 0.75; CASE$_{Ie}$: NMB = -3.02, R = 0.74
Dinghu, Feb. CASE$_{UOS}$: NMB = 6.60, R = 0.76; CASE$_{Ie}$: NMB = 7.67, R = 0.76
Tiyuxi, Mar. CASE$_{UOS}$: NMB = -6.63, R = 0.71; CASE$_{Ie}$: NMB = -7.66, R = 0.71
Dinghu, Mar. CASE$_{UOS}$: NMB = 3.22, R = 0.68; CASE$_{Ie}$: NMB = 4.06, R = 0.68
Tiyuxi, Apr. CASE$_{UOS}$: NMB = -8.53, R = 0.61; CASE$_{Ie}$: NMB = -9.99, R = 0.61
Dinghu, Apr. CASE$_{UOS}$: NMB = 8.02, R = 0.58; CASE$_{Ie}$: NMB = 8.92, R = 0.58
CASE$_{UOS}$
CASE$_{Ie}$
Observation
O$_3$ (μg/m^3)
0
70
140
210
280
01-01
01-05
01-09
01-13
01-17
01-21
01-25
01-29
02-01
02-01
02-05
02-09
02-13
02-17
02-21
02-25
03-01
03-01
03-05
03-09
03-13
03-17
03-21
03-25
03-29
04-01
04-01
04-05
04-09
04-13
04-17
04-21
04-25
04-29
05-01

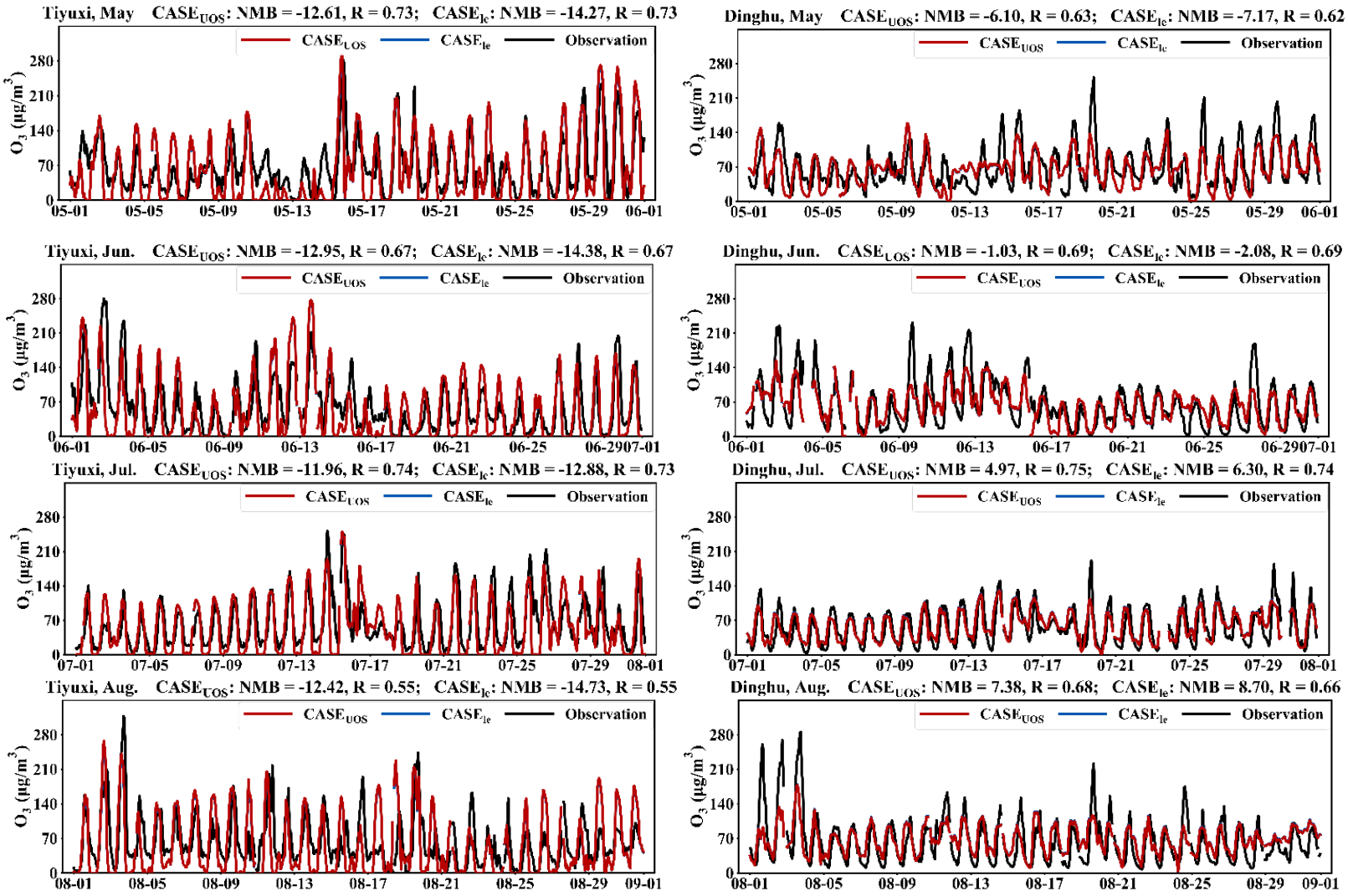
Tiyuxi, May CASE$_{UOS}$: NMB = -12.61, R = 0.73; CASE$_{Ic}$: NMB = -14.27, R = 0.73
Dinghu, May CASE$_{UOS}$: NMB = -6.10, R = 0.63; CASE$_{Ic}$: NMB = -7.17, R = 0.62
Tiyuxi, Jun. CASE$_{UOS}$: NMB = -12.95, R = 0.67; CASE$_{Ic}$: NMB = -14.38, R = 0.67
Dinghu, Jun. CASE$_{UOS}$: NMB = -1.03, R = 0.69; CASE$_{Ic}$: NMB = -2.08, R = 0.69
Tiyuxi, Jul. CASE$_{UOS}$: NMB = -11.96, R = 0.74; CASE$_{Ic}$: NMB = -12.88, R = 0.73
Dinghu, Jul. CASE$_{UOS}$: NMB = 4.97, R = 0.75; CASE$_{Ic}$: NMB = 6.30, R = 0.74
Tiyuxi, Aug. CASE$_{UOS}$: NMB = -12.42, R = 0.55; CASE$_{Ic}$: NMB = -14.73, R = 0.55
Dinghu, Aug. CASE$_{UOS}$: NMB = 7.38, R = 0.68; CASE$_{Ic}$: NMB = 8.70, R = 0.66
CASE$_{UOS}$
CASE$_{Ic}$
Observation
O$_3$ (μg/m^3)
0
70
140
210
280
05-01 05-05 05-09 05-13 05-17 05-21 05-25 05-29 06-01
06-01 06-05 06-09 06-13 06-17 06-21 06-25 06-2907-01
07-01 07-05 07-09 07-13 07-17 07-21 07-25 07-29 08-01
08-01 08-05 08-09 08-13 08-17 08-21 08-25 08-29 09-01

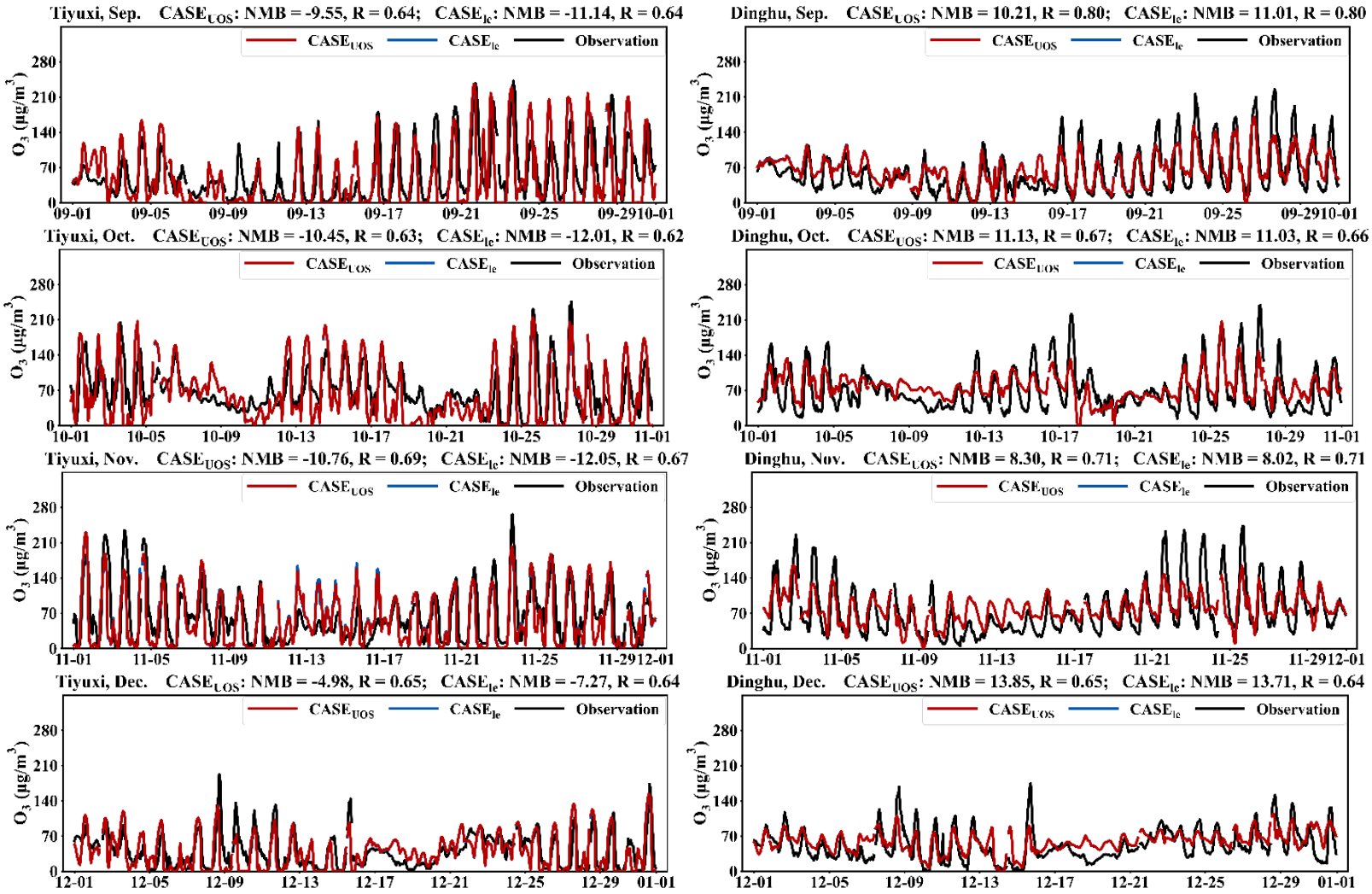

Fig. S21. Comparison of the observed and simulated hourly O_3 time series from $CASE_{le}$ and $CASE_{UOS}$ for each month in 2023 at Tiyuxi (left) and Dinghu (right), respectively.

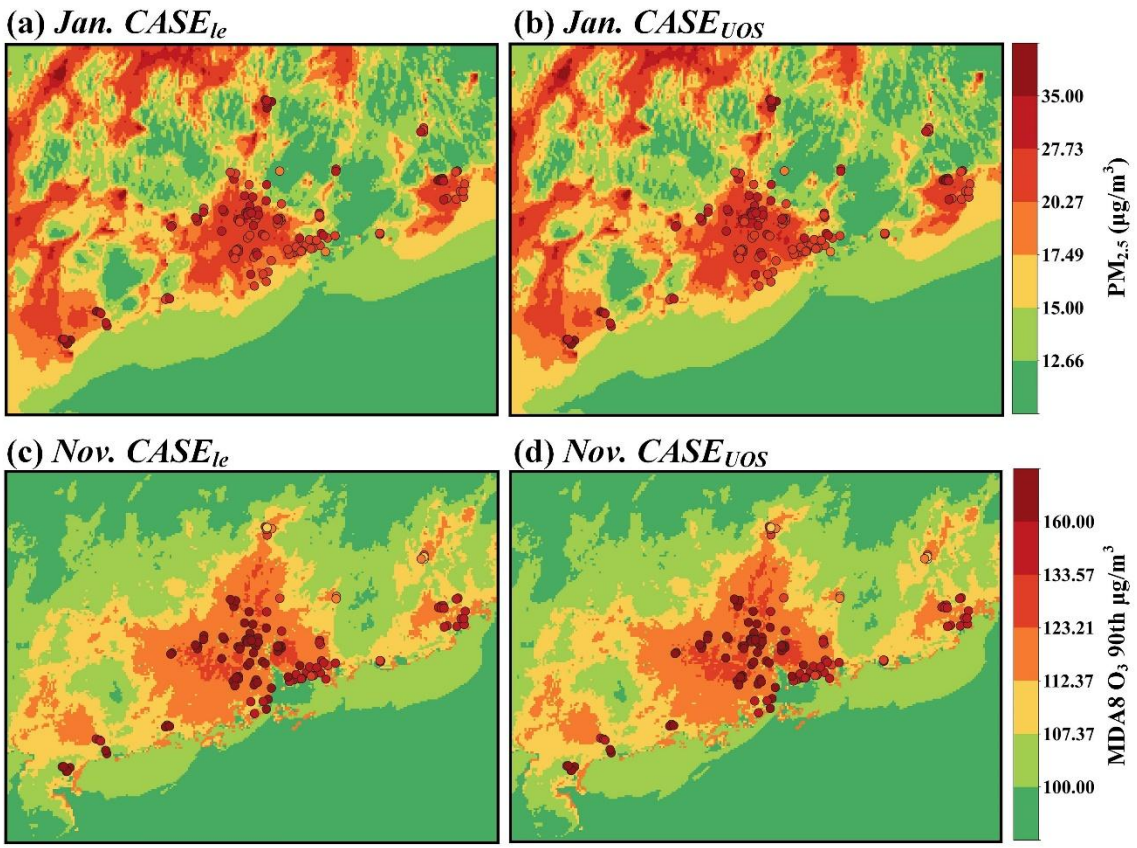

Fig. S22. Spatial distribution of the simulated monthly average surface $PM_{2.5}$ in January and the 90th percentile of the daily maximum 8h average O_3 (MDA8 O_3 90th) in November 2023 from $CASE_{le}$ (left) and $CASE_{UOS}$ (right) scenarios. Overlaid dots showed observed monthly average values from national air quality stations across Guangdong Province.

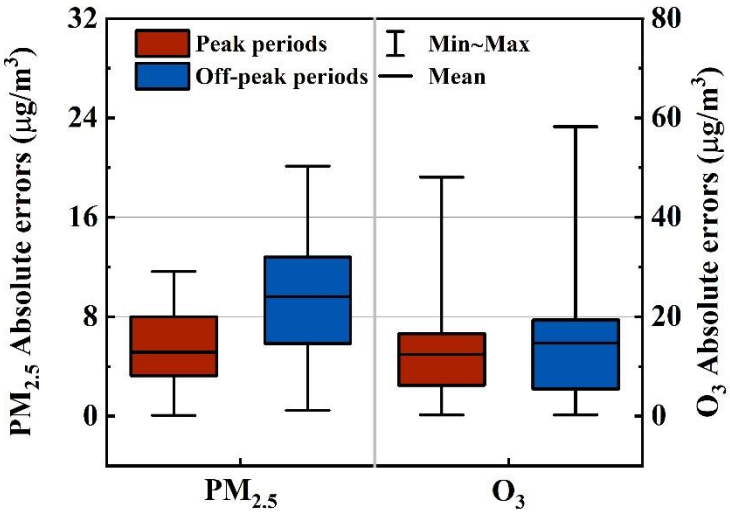

Fig. S23. The absolute errors for simulated $PM_{2.5}$ (left y-axis) and O_3 (right y-axis) using the updated emission inventory (EI_{UOS}) during emission peak and off-peak periods across all national monitoring stations in Guangdong Province.

To evaluate model performance during the peak hours of commercial cooking emissions, absolute errors of simulated $PM_{2.5}$ and O_3 against observations across all national monitoring stations in Guangdong Province were calculated and summarized separately for these peak periods and the remaining off-peak hours (**Fig. S23**). The analysis revealed that the absolute errors for $PM_{2.5}$ were substantially smaller overall during emission peaks, with the mean absolute error being 5.14 μg/m^3 compared to 9.60 μg/m^3 during off-peak hours. Moreover, the interquartile range narrowed considerably ([3.25, 7.98] μg/m^3 vs. [5.84, 12.80] μg/m^3), indicating that the updated inventory effectively constrained the temporal biases and uncertainties in $PM_{2.5}$ simulations during active emission period. The improvement for O_3 was relatively modest, with a mean absolute error of 12.41 μg/m^3 during peak periods, lower than the 14.76 μg/m^3 observed during off-peak periods. Overall, the updated emission inventory demonstrated better simulation capability during these high-emission windows, further validating the pronounced diurnal variation of commercial cooking emissions and underscoring the critical importance of accurately representing their temporal profiles to improve air quality model performance.

References

Center for Environmental Research Infromation Office of Research and Development U.S. Environmental Protection Agency Cincinnati (1999). Compendium Method TO-14:

Determination of Volatile Organic Compounds (VOCs) in Ambient Air Using Specially Prepared Canisters with Subsequent Analysis by Gas Chromatography

Huang J Z, Li W K, Zhang B C (2013). Study on Catering Source Emissions in Guangzhou (in Chinese): GUANGZHOU ENVIRONMENTAL SCIENCE, 1-2, 6

Huang X, Han D, Cheng J, Chen X, Zhou Y, Liao H, Dong W, Yuan C (2020). Characteristics and health risk assessment of volatile organic compounds (VOCs) in restaurants in Shanghai. Environmental Science and Pollution Research, 27(1): 490-499

Jin W J, Zhi G R, Zhang Y Z, Wang L, Guo S C, Zhang Y, Xue Z G, Zhang X M, Du J H, Zhang H, Ren Y J, Xu P, Ma J H, Zhao W J, Wang L F, Fu R C (2021). Toward a national emission inventory for the catering industry in China. Science of the Total Environment, 754: 142184

Liang X M, Chen L G, Liu M, Lu Q, Lu H T, Gao B, Zhao W, Sun X B, Xu J T, Ye D Q (2022). Carbonyls from commercial, canteen and residential cooking activities as crucial components of VOC emissions in China. Science of the Total Environment, 846: 10

Schauer J, Kleeman M, Cass G, Simoneit B (1999). Measurement of emissions from air pollution sources.: 1.: C1 through C29 organic compounds from meat charbroiling. Environmental Science & Technology, 33(10): 1566-1577

Sun C Y, Zhao L Y, Chen X, Nie L, Shi A J, Bai H H, Li G A (2022). A comprehensive study of volatile organic compounds from the actual emission of Chinese cooking. Environmental Science and Pollution Research, 29(35): 53821-53830

Wang H, Xiang Z, Wang L, Jing S, Lou S, Tao S, Liu J, Yu M, Li L, Lin L, Chen Y, Wiedensohler A, Chen C (2018). Emissions of volatile organic compounds (VOCs) from cooking and their speciation: A case study for Shanghai with implications for China. Science of the Total Environment, 621: 1300-1309

Yuan Y, Zhu Y, Lin C-J, Wang S, Xie Y, Li H, Xing J, Zhao B, Zhang M, You Z (2023). Impact of commercial cooking on urban $PM_{2.5}$ and O_3 with online data-assisted emission inventory. Science of the Total Environment, 873: 162256